TENNESSEE VALLEY AUTHORITY
CHATTANOOGA, TENNESSEE 37401
400 Chestnut Street Tower II

February 19, 1980

Director of Nuclear Reactor Regulation
Attention: Mr. L. S. Rubenstein, Acting Chief
Light Water Reactors Branch No. 4
Division of Project Management
U.S. Nuclear Regulatory Commission
Washington, DC 20555

Dear Mr. Rubenstein:

In the Matter of the Application of	)	Docket Nos. 50-390
Tennessee Valley Authority	)	50-391

On June 14-15, 1979, there was a meeting between TVA and the NRC on the Watts Bar Nuclear Plant containment buckling criteria. At this meeting with A. Hafiz and R. Lapinski of the NRC and NRC consultants Dr. Seide and Dr. Weingarten, TVA employees discussed additional requests for information which TVA received informally on May 14, 1979.

Enclosed are 40 copies of TVA's response to the requests for additional information as a result of this meeting.

Very truly yours,

TENNESSEE VALLEY AUTHORITY

L. M. Mills, Manager
Nuclear Regulation and Safety

Enclosure (40)

B001 S 40/40

8002260 716
a

WATTS BAR NUCLEAR PLANT

CONTAINMENT VESSEL
BUCKLING ANALYSIS

February 19,1980

Docket # 05000390
Control # 8002260716
Date 80/02/19 of Document
REGULATORY DOCKET FILE

Introduction

Before proceeding with the responses to the NRC questions, a brief description of the containment vessel follows. The containment is a low-leakage, free standing steel structure consisting of stiffened cylindrical walls with a hemispherical head. The stiffening is primarily circumferential; however, one of the vessel's lower bays is stiffened vertically. The circumferential stiffeners are spaced roughly four times Rt (10 foot intervals) and the vertical stiffeners are spaced at 5 degree intervals. Other locally stiffened areas are provided around the equipment hatch and two personnel locks. The base of the containment vessel is anchored in a concrete mat using pretensioned bolts on the inside and outside of the vessel extending down into the concrete mat. Equipment supported from the axisymmetric containment vessel include the personnel locks, equipment hatch and other minor attachments shown in Figure 1.

Figure 1 shows a schematic representation of the containment vessel geometry. Important information includes the shell thicknesses, vessel overall dimensions, ring locations, and the size of the stiffener rings. The location of the major supported equipment is also shown with dimensions roughly to scale.

Figure 2 shows a plot of the frequencies for the modes of natural vibration of the containment vessel. The natural frequency for the first and second axial modes for each of the Fourier harmonics of major interests are plotted.

NRC QUESTIONS

Question 1. Provide a description of the exact applied loads used for the buckling analysis. If any computer programs were used to obtain these loads, a complete description of the computer programs should be supplied. This description should include a discussion of the analytical and numerical methods used in the program, as well as a statement of its limitations and the methods used in its verification.

Response

The controlling load combinations for the buckling analysis are combinations No. 3 and No. 4 in section 3.8.2.3.2 of the Watts Bar FSAR. The hydrostatic and thermal loads in these combinations are not considered significant from a buckling standpoint and design internal pressure tends to increase the buckling strength. Therefore, for the buckling analysis dead weight and transient pressure loads were combined with Operating and Design Basis Earthquakes, since these combinations produce the greatest meridional and hoop compressive membrane stresses. For further discussion, see Appendix A.

A description of the computer programs used to determine loads is provided in our response to question 3. This description includes a discussion of program limitations and methods used. The Fourier series used to represent the specified asymmetric pressure transient was plotted for all elevations for representative transient times, and the plots were checked

against the TVA pressure curves. Fourier coefficients also were calculated by Anamet Labs and a cross check on the coefficients was made.

Question 2. Provide a description of how the buckling curves contained in the report were applied to the buckling of the containment vessel. The description should include the application of these buckling curves to asymmetric dynamic loads in the areas where penetrations are present.

Response.

Membrane stresses in the containment due to deadweight, seismic and transient pressure loads were calculated. The deadweight stresses were determined using hand calculations and seismic stresses were determined using the beam model described in our response to Question 6. An asymmetric transient load analysis was performed using a shell of revolution model for the pressure transients from all of postulated breaks.

The buckling analysis was performed using CBI computer program E1391. The maximum deadweight and earthquake stresses were combined with the transient load stresses at each of 40 timesteps, at 123 elevations and at 24 points around the vessel, evenly spaced at 15 degree intervals.

Figures 3.8B-1 through -10 in the Watts Bar FSAR were used to determine the critical buckling stress based on the containment vessel geometry. In general, these curves are based on theoretical and experimental results for buckling of shell structures. The shell bays between the stiffeners are considered as simplysupported cylinders and the vertically stiffened bay assumes panel buckling in determining critical buckling stress at a given elevation.

The interaction equations given in Appendix 3.8.B-4 and -5 of the FSAR were evaluated taking the summation of the stress ratios of compressive membrane to critical buckling stress times the buckling load factors in Table 3.8.B-2. These summations were investigated at each timestep azimuth and elevation described above. In this evaluation, the longitudinal membrane stresses produced by the asymmetric pressure transient load (NASPL) and horizontal earthquakes were considered as caused by bending loads in the interaction equations. Deadweight and vertical earthquake loads cause axial compression in the equations.

These interaction equations provide the criteria for evaluating the interaction of multi-axial compressive stress and hoop compressive stress. The maximum stress ratio summation considering all 24 points around the circumference was tabulated for each elevation for each interaction equation specified. In the areas where there were major penetrations which interrupt the basic stiffening scheme on the vessel, stiffeners were designed to carry the stresses in the shell around the opening.

Question 3. Provide in-depth description of all computer programs used in the buckling analysis. The description should

state the origin of the program, its limitations, and the methods used to verify its validity.

Response

Appendix B presents abstracts of the computer programs employed in the buckling analysis of the Watts Bar containment vessels. These abstracts provide a description of the each program and its limitations. CBI programs 1374 and E0781A and Anamet's BALL program were verified by comparison with results of programs in the public domain. The other programs were verified by comparison with the results of hand calculations. The dynamic shell analysis was done using CBI program 1374, which was developed by CBI from the Kalmins shell of revolution statics program. The results of this analysis were verified by the results of Anamet's analysis using the BALL program.

Question 4. Provide a description of the assumptions involved in modeling the containment vessel in order to use the programs identified in Question 3. This description should include a discussion of any convergence and/or accuracy checks that were made.

Response

The vessel was modeled as an axisymmetric shell of revolution. The circumferential stiffeners were modeled discretely as ring stiffeners. The section of the vessel that has vertical stiffening was modeled as an orthotropic shell.

The representation of the specified loads required a total of 21 Fourier harmonics. This Fourier representation included ten sine and ten cosine terms plus the axisymmetric loading. The vessel was assumed to be fixed at the base, and the mass of any supported equipment was smeared over the circumference at the appropriate elevation.

In addition to the usual convergence and accuracy checks used with shell of revolution models, a completely independent analysis was done by Anamet Laboratories using a completely different computer program and model for one of the specified pressure transients. A comparison of the 1374 results with the Anamet results for a similar vessel geometry is shown in Figures 3a and 3b.

Question 5. Provide a complete step-by-step description of which and how the buckling stress criteria were applied.

Response

The buckling criteria in Appendix 3.8B of the FSAR was applied to the Watts Bar Containment design. The step-by-step approach used for the application of these criteria has been described in our response to Question 2 and in Appendix A.

Question 6. Explain the procedure of obtaining the stress distribution in the shell using lumped mass beam model instead of a shell model for the dynamic seismic analysis.

Response

The Timoshenko shear beam is a realistic analog for the response of a shell of revolution to seismic ground motion. A complete discussion of the use of the beam model for the seismic analysis of containment vessel is provided in Appendix C. "The Design of a Thin Shell Nuclear Containment Vessel for Seismic Loading" by Jon Hagstrom.

Question 7. Explain the justification for using an axisymmetric geometry computer program for the containment vessel.

Response

The main aspects of the containment geometry that are not handled precisely by the shell of revolutions model are the vertical stiffening and the attached equipment, primarily the locks and hatch. The spacing of the vertical stiffening used for the Watts Bar containment vessel is such that the orthotropic representation is a very reasonable one. This can be verified by results in the literature or static analysis.

For the attached equipment, some additional consideration is necessary. In the analysis of the Watts Bar containment vessel this aspect was handled by doing a separate dynamic analysis for the response of the locks and hatch. The procedure for doing this additional analysis is spelled out in the FSAR, Par. 3.8.2.4.7. In effect, the locks and hatch are treated as a supported subsystem and they are evaluated using a separate dynamic model. This general approach is commonly used in the dynamic analysis of nuclear plants.

Question 8. Provide the criteria used in the computer program to calculate the buckling loads, description of the mass matrix formulation and how the maxima at each time point were chosen in the CBI containment shell analysis using the finite element model.

Response

The criteria used in the bucking program is described in our response to Question 2 and in Appendix A. As discussed, for each timestep 24 locations around the circumference were considered at each elevation investigated.

The mass matrix formulation for the 1374 program is described in the program abstract for 1374 in Appendix B.

Question 9. Explain in detail the criteria and its justification for determining the interaction effects between the containment shell and the attached equipment.

Response

As described above, interaction effect between the containment shell and the attached equipment was determined by doing a separate analysis for the supported system. A time history response of the motion of the axisymmetric shell at the point of

attachment of a supported system was determined from the shell of revolution results. A response spectra for this calculated motion was generated; the frequencies of the supported system was calculated; and a spectral response was calculated.

An experimental and theoretical investigation of mass loading effects has been reported by North American Rockwell Corporation in Report SD 68-29. Excerpts from this report are included in Appendix "D" of this response.

Question 10. Was a thermal analysis conducted? If the answer is yes, describe step by step the procedure that was followed.

Response

Two thermal analyses were performed on the containment vessel. One analysis was an axisymmetric thermal of the embedment region to investigate the effect of the base restraint. This analysis utilized axisymmetric elements to model the lower containment region with the temperature distribution shown in Figure 3.8A-2 of the FSAR. Figure 4 shows the summation of stresses due to coincident loads.

The other thermal analysis was an asymmetric analysis of the containment vessel using an axisymmetric shell of revolution model. The temperature distribution varies significantly in the circumferential and vertical directions 1000 seconds after the pressure transient (LOCA) creating internal stresses in containment from self-constraint. Fourier representations were used to simulate the circumferential temperature distribution. A step-by-step discussion of this analysis is given in Appendix E.

The stresses observed from these analyses are significantly less than the ASME allowable stress intensities. Therefore it can be determined by observation that buckling is not a problem.

Question 11. Provide a list of all the loading combinations and the stress allowables (stress intensity and buckling stress) which had been used in the design of the steel containment.

Response

The loading combinations used in the design of the containment vessels are given in Section 3.8.2.3.2 of the FSAR.
TAble 3.8.2-1 in the FSAR gives the allowable stress criteria for these loading combinations. Appendix 3.8B of the FSAR give the allowable buckling criteria for all loading combinations.

Question 12. Indicate the critical loading combinations which control the design of the steel containment shell with regard to stress intensity and buckling. Identify also the regions and/or regions of the steel containment which was controlled by these critical loadings.

Response

Only those loading combinations with pressure transients (NASPL) govern the shell with regard to stress intensity and/or buckling. See attached Figures 5 and 6 for a summary.

Question 13. Indicate, approximately, the contribution (as a percentage of the allowable stress intensity and allowable buckling loads) of each of the loadings identified in Question 12.

Answer

Refer to figures 5 and 6. Percentages are in parenthesis.

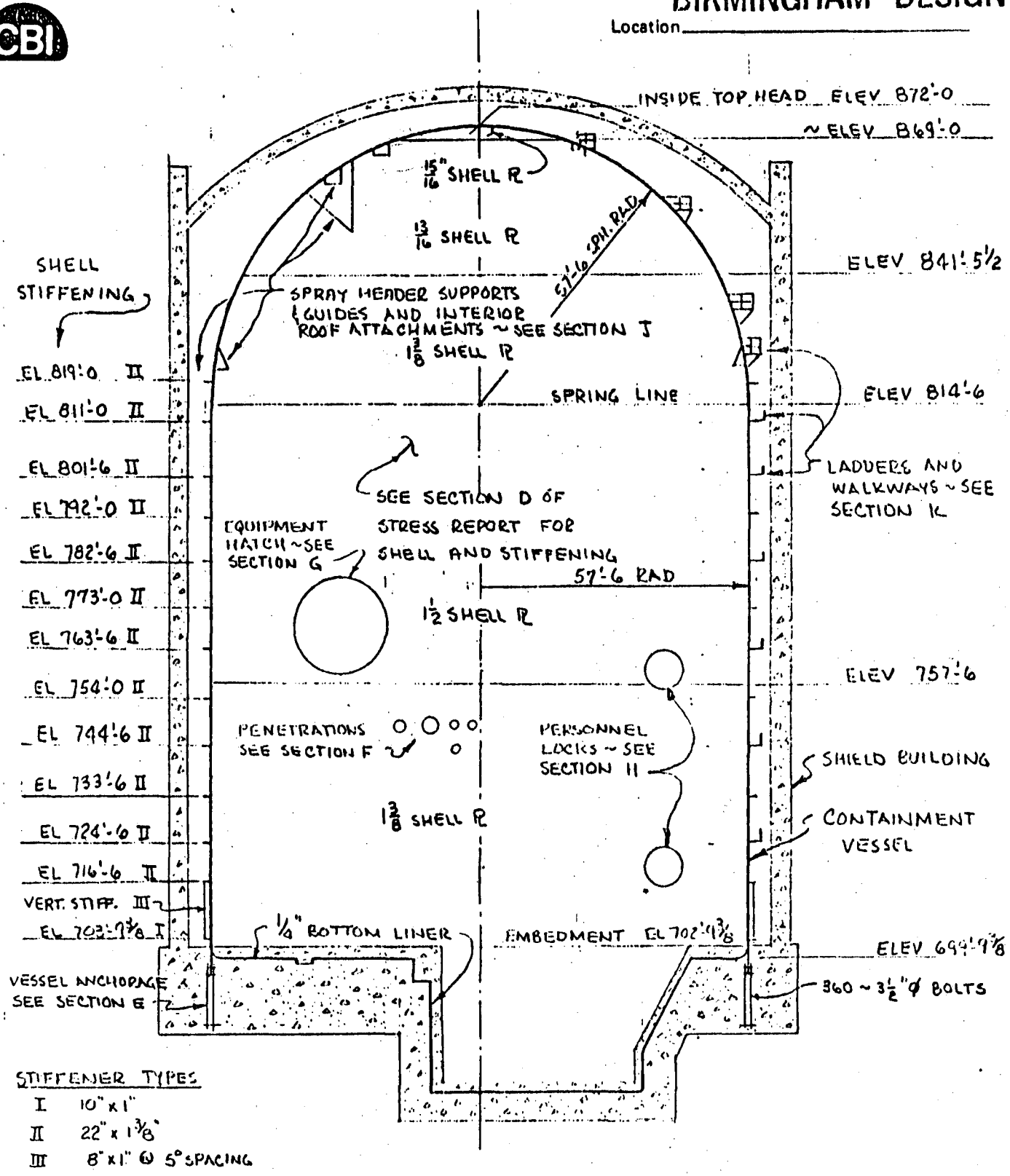

FIGURE 1
SECTION THRU VESSEL

SUBJECT	MADE BY	CHKD BY	REV	By		CHARGE NO.
INTRODUCTION	REI	WLL		Chkd		72-4333
	DATE 10-4-7	DATE 10-16-74		Date		A-3 SHT OF

Location

TVA WATTS BAR CONTAINMENT VESSEL

MODEL 6 FREQUENCIES

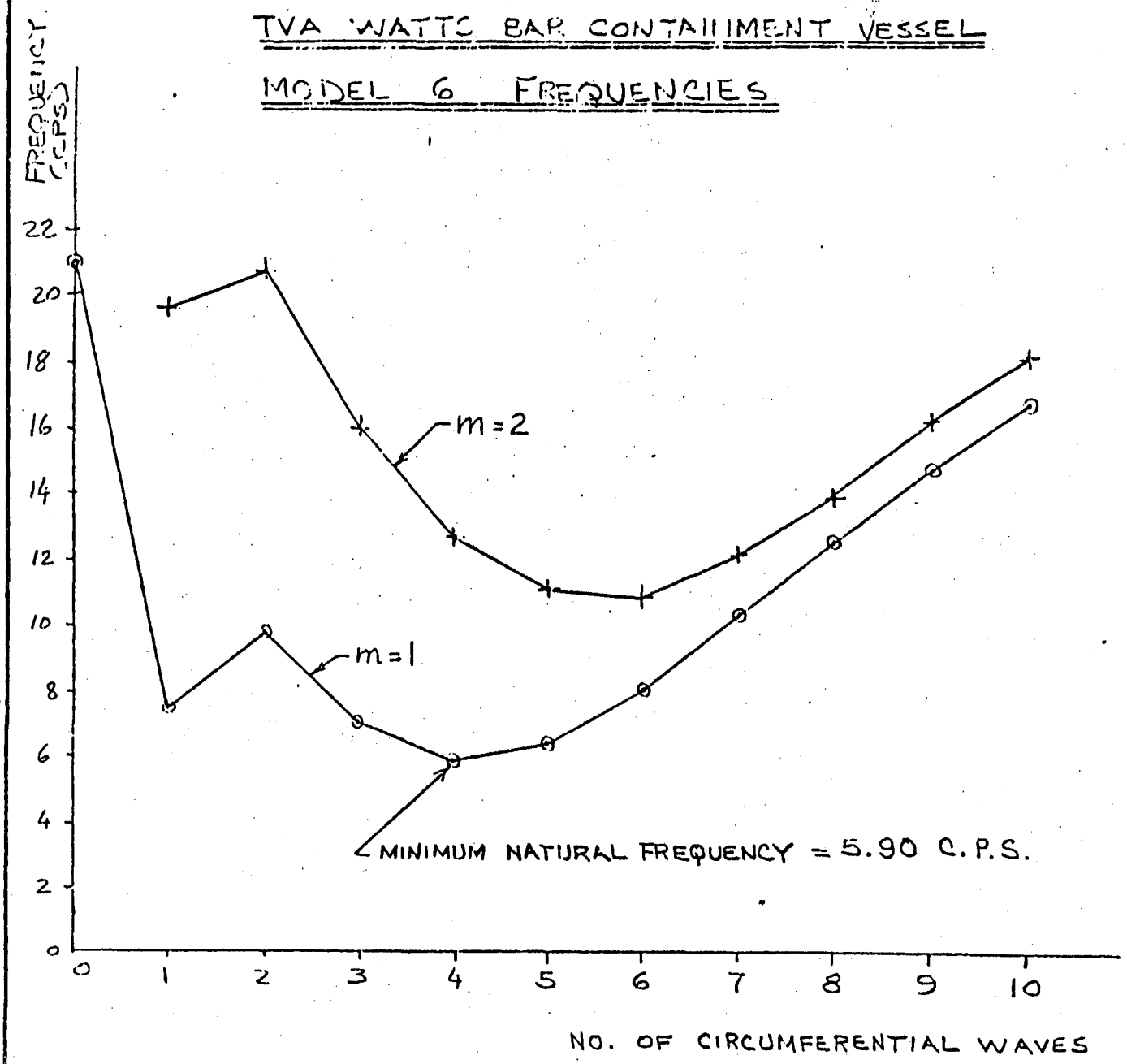

(m REFERS TO LONGITUDINAL MODE SHAPES)

FIG. 2

SUBJECT	MADE BY	CHKD BY	REV	By		CHARGE NO.
TRANSIENT ANALYSIS	FES	C.J.P.		Chkd	*	724333
WATTS BAR CONTAINMENT	DATE 2/74	DATE 2/74		Date		DWG SHT

CBI

Location

BRK IN ELEMENT 3

MAXIMUM COMPRESSIVE VALUE OF LONGITUDINAL FORCE VS ELEVATION

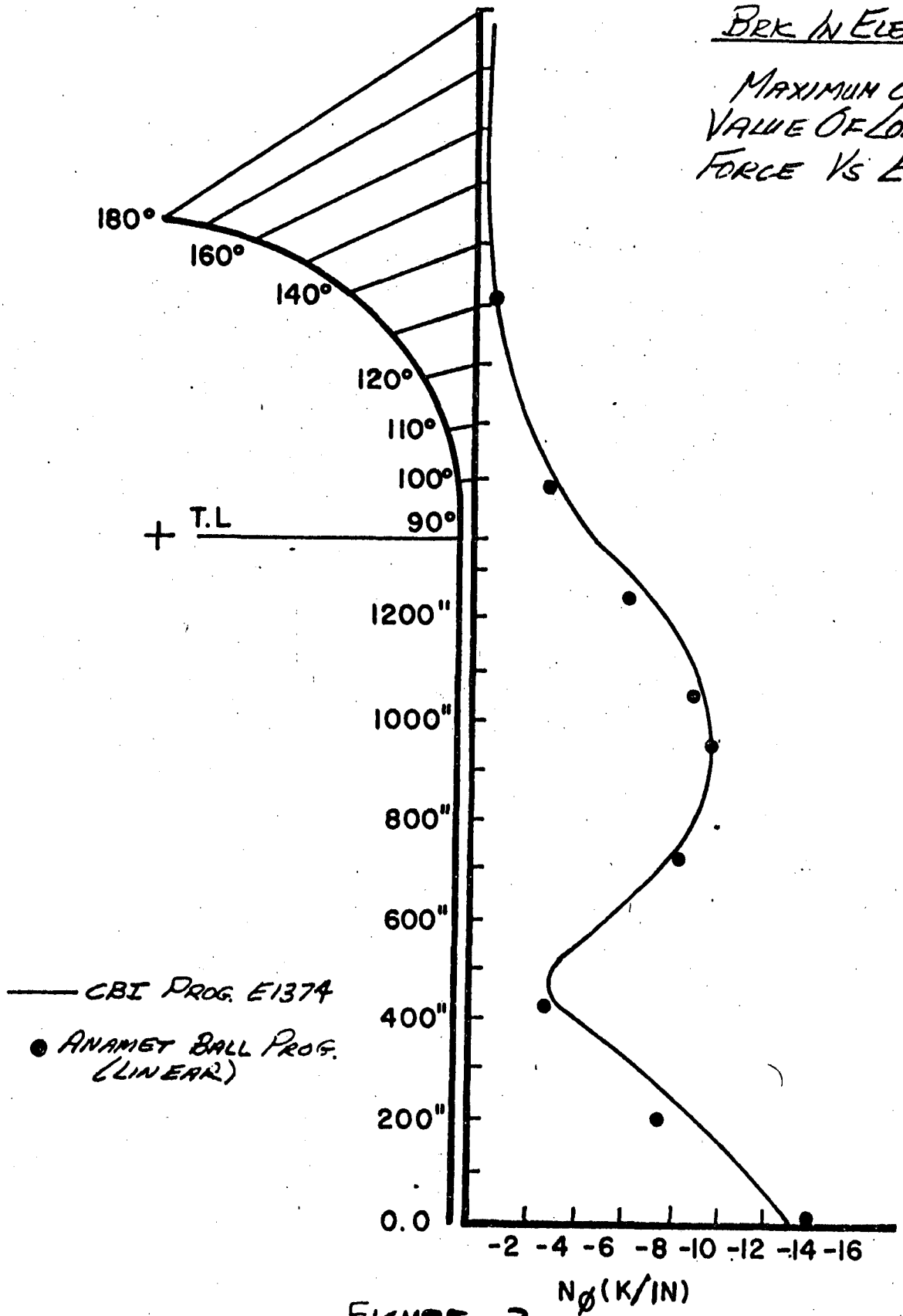

FIGURE 3a

SUBJECT	MADE BY	CHKD BY	REV			CHARGE NO.
FIG 7	[illegible]	TES		By		69-5545
SEQUOYAH CONTAINMENT	DATE 10/73	DATE 10/73		Chkd		BN25
				Date		SHT ___ OF ___

QO 64 REV 4-73

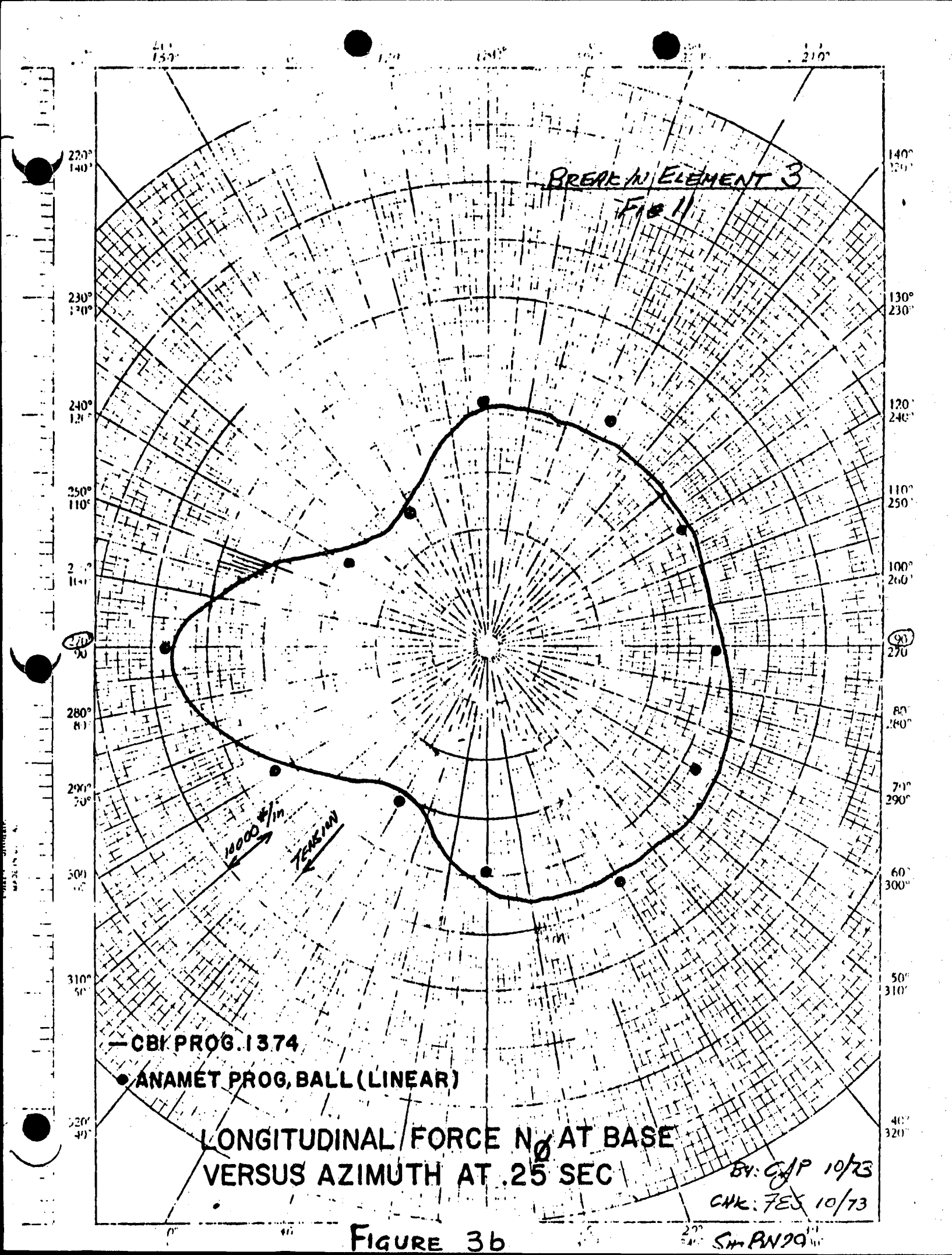
BREAK IN ELEMENT 3
FIG 11
10000 #/in
TENSION
—CBI PROG. 1374
• ANAMET PROG. BALL (LINEAR)
LONGITUDINAL FORCE N$_\phi$ AT BASE
VERSUS AZIMUTH AT .25 SEC
BY: CJP 10/73
CHK: FES 10/73
SHT RN29

FIGURE 3b

GO 54 REV 8-72

CB

LOCATION OF OUTPUT POINTS

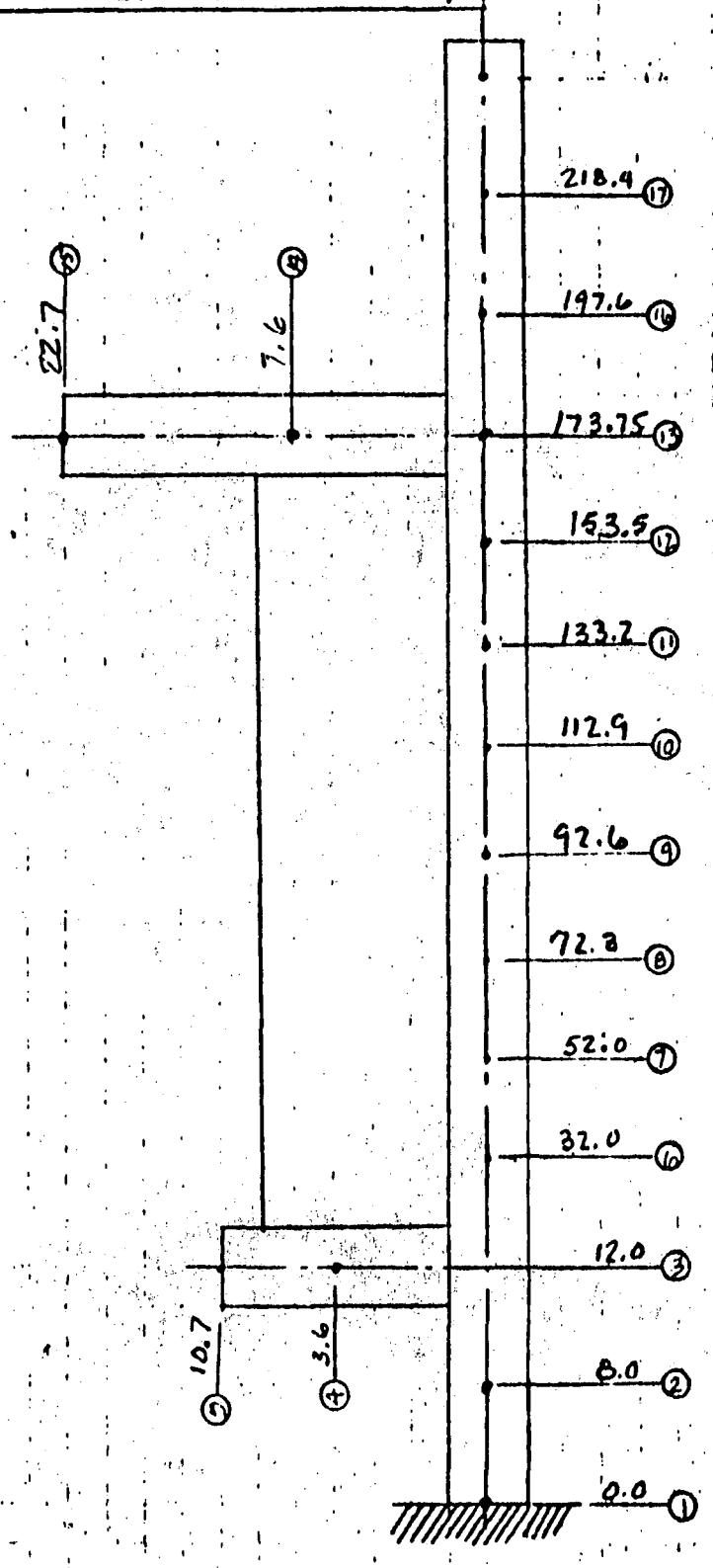

Location BIRMINGHAM DESIGN

σ_φ	σ_θ	w
3382	6581	.9954
3382	6427	.9916
3382	6947	1.005
3383	8024	1.035
	8532	1.052
	7668	1.035
	4637	.9629
	-1093	.8204
	-5561	.6086
	13240	.3549
3382	2568	.0891
	704	.0430
	-1034	.0

Fig 4

SUBJECT	MADE BY DMB	CHKD BY PEA	REV	By		CHARGE NO. 72-4333
	DATE	DATE		Chkd		

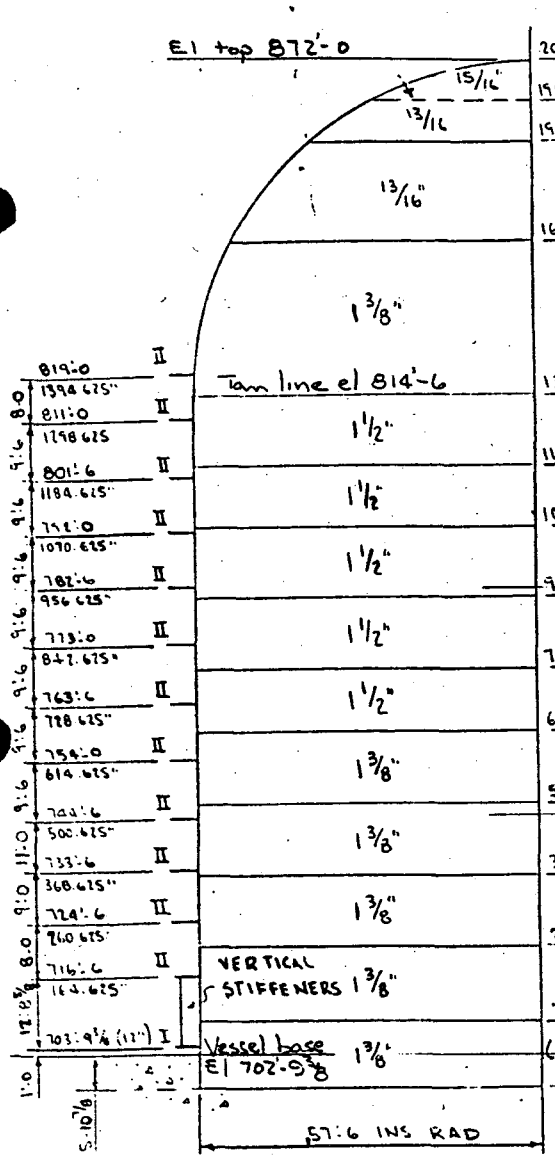

	DL + 1/2 SSE Stress Int	NASPL Stress Intensity	Az / Time	Remarks.
	.196	2033	315°/.21	BREAK IN HL # 3
	(5%) 541	(29%) 5469	300°/.24	BREAK IN HL # 3
	(2%) 344	(47%) 9009	300°/.24	BREAK IN HL # 3
	(4%) 690	(73%) 14050	285°/.14	BREAK IN HL # 1
	(5%) 1110	(97%) 18400	300°/.14	Break in HL # 1 (Allowable = 19250 psi)
	(8%) 1540	(92%) 17760	315°/.23	Break in HL # 4

Fig 5
GOVERNING STRESS INTENSITIES
(Allowable = 1.1 Sm = 19250 psi)

WM 1 of 1
6/8/79

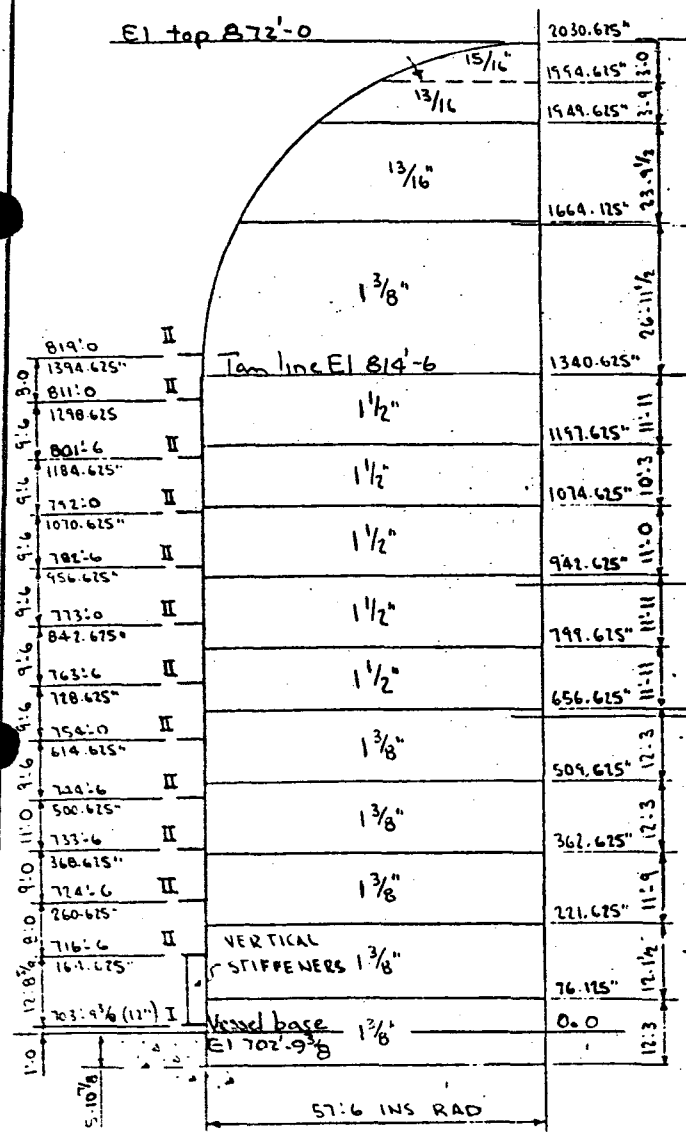

Combination	Ratio	Azimuth/Time	Remarks
AXIAL + BEND	(91%) .91	270/.22	BREAK IN HL # 4
AXIAL + BEND	(90%) .90	270/.24	BREAK IN HL # 3
AXIAL + BEND	(85%) .85	270/.24	BREAK IN HL # 3
AXIAL + BEND + TORS	(84%) .84	270/.24	BREAK IN HL # 3
Axial + bend + Tors	(96%) .96	225/.13	Break in HL # 6

FIG 6
GOVERNING BUCKLING RATIOS

WM 1 of 1
6/8/79

LIST OF APPENDICES

Appendix A - "Discussion of Buckling Analysis," Section DCA, Watts Bar Stress Report

Appendix B - "Description of Computer Programs" - Section C, Watts Bar Stress Report

Appendix C - "The Design of a Thin Shell Nuclear Containment Vessel for Seismic Loading" by Jon Hagstrom

Appendix D - "Mass-Loading Effects on Vibration of Ring and Shell Structures" by S. Y. Lee, S. S. Tang, and J. G. Liyeos, North American Rockwell SD 68-29, dated February 1968.

Appendix E - "Effect of Nonsymmetric Thermal Loading on Shell" - Appendix G, Watts Bar Stress Report

APPENDIX A

Discussion of Buckling Analysis

DISCUSSION OF BUCKLING ANALYSIS

This section presents the buckling analysis of the Watts Bar Containment Vessel for the pressure transient loading condition. This buckling analysis is performed in accordance with TVA Specification 1440.

Shell loads for the buckling analysis are developed in the section presenting the pressure transient shell analysis. In addition to these pressure transient loads, this analysis also considers the effects of the shell weight, miscellaneous loads, and loads resulting from vertical and horizontal seismic action.

The buckling analysis is performed using CBI computer program E1391. The pressure transient loads developed by the pressure transient shell analysis are stored by the computer and then read in directly by program E1391. The other loads considered in the buckling analysis are derived in various portions of the analysis of the containment vessel. These loads are assembled and input separately into the program. The geometry of the vessel describing the shell and stiffening and the material properties are also read into the program.

The program performs the buckling analysis for the vessel at each point considered in the pressure transient shell analysis. For the Watts Bar Containment Vessel the following points are checked:

6 Hot Leg Breaks (½ SSE)

6 Cold Leg Breaks (½ SSE)

1 Hot Leg Break (SSE)

123 Elevations for each break

24 Azimuths for each elevation

40 Timesteps for each azimuth

The analysis is performed using all of the breaks for the one-half safe shut down earthquake (½ SSE) and for one break for the safe shut down earthquake (SSE). It can be noted that by comparing the results of the buckling analysis for

the SSE break with the corresponding break using ½ SSE the buckling ratios are larger for the ½ SSE condition. The load factor ~~of safety~~ for the ½ SSE condition is 1.25 while for the SSE condition it is 1.1. Since the seismic loads are small compared to the pressure transient loads it can be seen that the ½ SSE condition is the critical condition. The one SSE condition is reported to confirm this fact and it is not necessary to investigate any other breaks for the SSE condition.

The pressure transient loads are input at each point under consideration while the other loads are input at fewer locations. The program performs a linear interpolation to obtain the values of these other loads at each point where the buckling stress is calculated.

In order to determine the critical buckling stress at any point, it is necessary to determine the vessel geometry in the region of that point. The program considers several cases depending on the shell and stiffening arrangement. Once the geometrical properties are determined the program calculates the critical buckling stress in accordance with Appendix H, Revision 1 of TVA Specification 1440.

By multiplying the actual stress by the load factor ~~of safety~~ and dividing the product by the critical buckling stress the buckling ratio is determined. The buckling ratio is calculated for meridional stresses due to axial and bending loads, circumferential stress, and shear stress. These individual buckling ratios are then combined to form the final buckling ratios in accordance with Appendix H.

For each elevation under consideration the program calculates the ratios for all azimuths and times and finds the maximum buckling ratio. This ratio, with its corresponding azimuth and time is then recorded.

A further discussion of the methods used may be found on the following pages.

CBI

Location Birmingham

Description of Program E13910

Shell Buckling Analysis for TVA Containment Vessel

Introduction

Program #13910 performs the buckling check of the TVA ice condenser containment vessel for Non-axisymmetric pressure loading combining with the dead loads and seismic loads occuring in the vessel. The non-axisymmetric loads are developed by CBI program E1374. The resulting stresses are compared to critical buckling stress and by using a specified factor ~~of safety~~ the buckling ratio is found.

Calculation of Dead Loads and Seismic Loads

As a general rule, dead loads and seismic loads are calculated at a few points along the vessel and the vessel is checked for buckling at many more points. As a result the program performs a linear interpolation to derive the dead loads and seismic loads at any given point along the vessel.

Calculation of Critical Buckling Stresses

In order to determine the critical buckling stress at a given point it is necessary to determine the geometry in the region of that point. The program considers four cases:

a) cylinders stiffened meridionally and circumferentially
b) cylinders stiffened circumferentially
c) spheres stiffened circumferentially and meridionally
d) unstiffened spheres

For each of these conditions certain constants must be determined based on known geometry. This information is in the form of graphs and is input into the computer as a series of straight lines. Once these constants are known, the critical buckling stresses can be determined using the applicable formulae. These calculations are based on Appendix H of TVA specification 1440.

Calculation of Stress and Buckling Ratios

The program calculates stresses and buckling ratios at any number of elevations and azimuths and for any number of time periods and then finds the maximum buckling ratio at each elevation. The program calculates four stresses at each point:

a) meridional stress due to axial loads
b) meridional stress due to bending loads
c) circumferential stress
d) shear stress

The program considers only compressive stresses. If a stress is tensile it is set equal to zero. For each of the stresses a buckling ratio is calculated using the stress multiplied by a factor of safety and divided by the critical buckling stress. These buckling ratios are then combined and five ratios result:

a) Axial + Circumferential
b) Axial + Bending
c) Axial + Shear
d) Axial + Shear + Bending
e) Axial + Shear + Circumferential

After these combined ratios are calculated, the maximums regardless of time or azimuth are recorded for each elevation.

In areas where vertical stiffening is present the program calculates the buckling ratio of the stiffener acting with the shell as a column simply supported at each end. The portion of the shell used in the column is determined using the rules of the Shell Analysis Manual referenced in Appendix H of Specification 1440. The buckling ratio is calculated in the manner discussed previously and the maximum is recorded.

Program Output

The program prints out the following data at each elevation considered:

a) Basic shell data and geometry of stiffeners
b) Load such as static pressure, dead loads, and seismic loads
c) Buckling stress coefficient
d) The five combined buckling ratios.
e) Vertical stiffener buckling ratios

APPENDIX B

Description of Computer Programs

SECTION C

DESCRIPTION OF COMPUTER PROGRAMS

COMPUTER PROGRAMS USED BY CBI

1374	SHELL DYNAMIC ANALYSIS PROGRAM } Modified Kalmin
E0781A	SHELLS OF REVOLUTION PROGRAM } Modified Kalmin
1017	MODAL ANALYSIS PROGRAM
E1622	LOAD PREPROCESSOR FOR 1374
E1623	POST PROCESSOR FOR E1374
E1624	SPECTRAL CURVE GENERATOR
E1391Φ	SHELL BUCKLING ANALYSIS PROGRAM
E1668	SPECTRAL ANALYSIS FOR ACCELERATION RECORDS

COMPUTER PROGRAMS USED BY ANAMET

PROGRAM BALL ANALYSIS OF NONLINEAR DYNAMIC SHELLS OF REVOLUTION

PROGRAM E1374 10/31/73

1. Introduction

Program E1374 is CBI's shell dynamic analysis program. Presently, it is capable of extracting eigenvalues and performing undamped transient analysis. Non-axisymmetric loads can be handled through the use of appropriate Fourier series.

The equation of motion for a particular Fourier harmonic n of an undamped system is

$$[M_n]\{\ddot{U}_n\} + [K_n]\{U_n\} = \{P_n\}$$

where
$[M_n]$ = Mass matrix
$[K_n]$ = Stiffness matrix
$\{P_n\}$ = Applied load
$\{U_n\}$ = Displacement
$\{\ddot{U}_n\}$ = Acceleration

Note that all of the above are functions of n.

In order to calculate free vibration frequencies and mode shapes the applied load is set equal to zero, $\{U_n\}$ is assumed to be a harmonic function of time, and the eigenvalues and eigenvectors of the resulting equation obtained using the method shown in Section 4.

If the transient response due to a time-varying load is required, the numerical integration technique outlined in Section 5 is used.

2. Stiffness matrices*

In general the procedure for forming the stiffness matrices is to first find influence values for each segment (or element) using Runge-Kutta numerical integration and then manipulate these values mathematically as follows:

Starting with the influence values

$$\{U_2\} = [Y_1]\{U_1\} + [Y_2]\{F_1\} + \{Z_1\}$$
$$\{F_2\} = [Y_3]\{U_1\} + [Y_4]\{F_1\} + \{Z_2\}$$

which are obtained by setting each element of $\{U_1\}$ and $\{F_1\}$ to one in succession, while all the other elements of these vectors are zero, and integrating the thin shell differential equations to the other end of the segment. The vectors $\{Z\}$ are obtained by setting $\{U_1\} = \{F_1\} = \{0\}$ while applying the distributed loads and integrating to the end of the segment.

To change this to stiffness matrix form, one needs only switch $\{F_1\}$ and $\{U_2\}$, thus

$$\{F_1\} = [K_1]\{U_1\} + [K_2]\{U_2\} + \{C_1\}$$

$$\{F_2\} = [K_3]\{U_1\} + [K_4]\{U_2\} + \{C_2\}$$

* See References (1) and (2)

where $\{F_1\}$ = forces at start of segment

$= \{Q, N\phi, M\phi, N\}_{@1}$

$\{F_2\}$ = forces at end

$\{U_1\}$ = displacements at start of segment

$= \{W, U\phi, \beta\phi, U_\theta\}_{@1}$

$\{U_2\}$ = displacements at end

$[K_1] = [-Y_2^{-1}Y_1]$

$[K_2] = [Y_2^{-1}]$

$[K_3] = [Y_3 - Y_4Y_2^{-1}Y_1]$

$[K_4] = [Y_4Y_2^{-1}]$

$\{C_1\} = \{Y_2^{-1}Z_1\}$

$\{C_2\} = \{Z_2 - Y_4Y_2^{-1}Z_1\}$

Since Program 1374 is not set up to handle longitudinal stiffeners, the integration for this portion of the shell is performed using Program 781. The influence values are then converted to stiffness matrix form and stored on disc. After Program 1374 has set up the stiffness matrices for the unstiffened shell, the matrices for segments with stiffening are replaced with the Program 781 matrices from disc. The solution in Program 1374 then continues in the standard manner. This consists of assembling the overall stiffness matrix $[Kn]$ and load vector $\{Cn\}$, reducing to upper triangular form, and back-substituting.

3. Ring Matrices

In order to develop a stiffness matrix for the ring stiffeners the following assumptions were made:

1. Thin beam theory is applicable, i.e. a normal to the neutral axis remains straight and normal after deformation and the thickness in negligible compared to the radius.

2. The stiffness of the ring out of its plane is negligible.

3. The ring is attached to a cylinder.

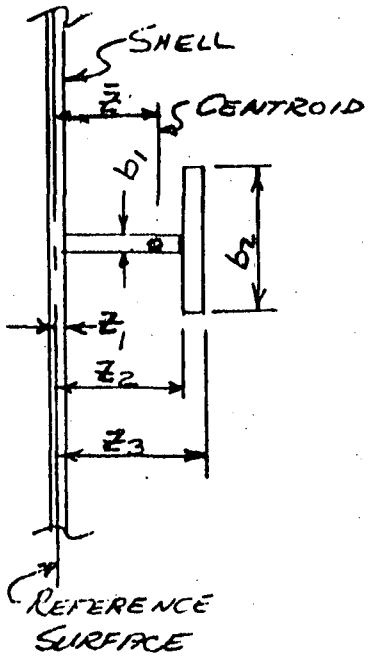

FIG. 1

4. The ring is made of one isotropic material with Poisson's ratio zero.

5. The ring can be divided into a series of cylinders of constant thickness. (See Fig. 1)

The ring is then treated as a series of m layers which start a distance Z_i from the reference surface, which is the mid surface of the shell, and ends at Z_{i+i}. The width of the layer is b_i. Then using the equations from Kalnin's paper*:

* See Reference (3).

$$A = \sum_{i=1}^{m} b_i (Z_{i+i} - Z_i)$$

$$A\bar{Z} = \frac{1}{2} \sum_{i=1}^{m} b_i (Z_{i+i}^{\ 2} - Z_i^{\ 2})$$

$$I = \frac{1}{3} \sum_{i=1}^{m} b_i \ (Z_{i+i}^{\ 3} - Z_i^{\ 3})$$

where A = area of section

$\bar{Z}$ = centroid of section, measured from reference surface

I = moment of inertia of section about reference surface

and

$$M_{\theta n} = EIk_{\theta n} + EA\bar{Z}\ e_{\theta n} \qquad (1)$$

$$N_{\theta n} = EA\ e_{\theta n} + EA\bar{Z}\ k_{\theta n} \qquad (2)$$

$$e_{\theta n} = \frac{1}{r}\ (nu_{\theta n} + w_n) \qquad (3)$$

$$k_{\theta n} = \frac{n}{r^2}\ (n\ w_n + u_{\theta n}) \qquad (4)$$

where

$(\ )_n$ = amplitude of a variable with n circumferential waves, e.g. $M_\theta = M_{\theta n} \cos n\theta$.

$M_{\theta n}$ = moment about the reference surface

$N_{\theta n}$ = thrust in ring

$e_{\theta n}$ = strain at reference surface

$k_{\theta n}$ = curvature

w_n = radial displacement of reference surface

$u_{\theta n}$ = circumferential displacement of reference surface

r = radius of reference surface

E = modulus of elasticity

Note that the equations above assume that all variables except $u_{\theta n}$ vary as cos $n\theta$. The equations also apply to sine series but the sign of n must be changed.

The potential energy of the ring is:

$$V = \int_0^{2\pi} \left[\frac{1}{2}\left(M_\theta k_\theta + N_\theta e_\theta\right) + Qw + Nu_\theta \right] r d\theta$$

where Q = radial force on ring at reference surface
N = circumferential force on ring at reference surface

Performing the integration, after having expanded the displacements and forces into Fourier series, yields

$$V = \pi r \sum_{n=0}^{\infty} \left[\frac{1}{2}\left(M_{\theta n} k_{\theta n} + N_{\theta n} e_{\theta n}\right) + Q_n w_n + N_n u_{\theta n} \right] \qquad (5)$$

since $\int_0^{2\pi} \sin n\theta \cos m\theta \, d\theta = \int_0^{2\pi} \sin n\theta \sin m\theta \, d\theta =$

$$= \int_0^{2\pi} \cos n\theta \cos m\theta \, d\theta = 0 \text{ if } n \neq m$$

Substituting egs. (1) to (4) into eq. (5), yields:

$$V = \pi r \sum_{n=0}^{\infty} \left\{ \frac{EA}{r^2} \left[\frac{1}{2} \frac{I}{Ar^2} (n^2 w_n + n u_{\theta n})^2 + \right.\right.$$

$$\left. + \frac{\bar{Z}}{r} n(n w_n + u_{\theta n})(w_n + n u_{\theta n}) + \frac{1}{2}(n u_{\theta n} + w_n)^2 \right] +$$

$$\left. + Q_n w_n + N_n u_{\theta n} \right\}$$

Since $\frac{\delta V}{\delta w_n} = \frac{\delta V}{\delta u_{\theta n}} = 0$, then

$$Q_n = \frac{-EA}{r^2} \left\{ \left[1 + \frac{\bar{Z}}{r} 2n^2 + \frac{I}{Ar^2} n^4 \right] w_n + n \left[1 + \frac{\bar{Z}}{r} (n^2+1) + \frac{I}{Ar^2} n^2 \right] u_{\theta n} \right\} \quad (6)$$

$$N_n = \frac{-EA}{r^2} \left\{ n \left[1 + \frac{\bar{Z}}{r} (n^2+1) + \frac{I}{Ar^2} n^2 \right] w_n + n^2 \left[1 + 2\frac{\bar{Z}}{r} + \frac{I}{Ar^2} \right] u_{\theta n} \right\} \quad (7)$$

For each ring, A, I, and $\bar{Z}$ (See Fig. 1) are input directly into the program. The stiffness terms are then calculated using equations (6) and (7).

In order to develop a mass matrix it was assumed that the ring behaved as though it were a lump mass located at the reference surface but including rotational inertia proportional to its eccentricity. This yields a simple diagonal mass matrix.

$$\rho A \begin{bmatrix} 1. & & & \\ & 1. & & \\ & & \bar{z} & \\ & & & 1. \end{bmatrix} \begin{bmatrix} w_n \\ u_{\phi r} \\ \beta_{\phi n} \\ u_{\theta n} \end{bmatrix}$$

where ρ = mass density of the ring material.

These mass and stiffness matrices are then added to the gross matrices as they are assembled.

4. Natural Modes and Frequencies

The eigenvalues are extracted using an iterative procedure*. In order to avoid time consuming integration at each iteration, the influence of 8 independent loading systems is determined before the iterative procedure starts. The results of each loading system are converted to $\{C_1\}$ and $\{C_2\}$ as per above, and these vectors constitute a column of the influence value matrix $|B|$. The loading systems used, in order, are:

Col. 1- $P_n = 1 - \xi^2(3-2\xi)$

2- $P_\ell = 1 - \xi$

3- $P_n = -\xi\,(1-2\xi + \xi^2)/L$

4- $P_c = 1 - \xi$

5- $P_n = \xi^2(3-2\xi)$

6- $P_\ell = \xi$

7- $P_n = \xi^2(1-\xi)/L$

8- $P_c = \xi$

where L = length of segment

ξ = S/L

S = coordinate along meridian

P_n = normal pressure

P_ℓ = longitudinal load

P_c = circumferential load

(* See Ref. (4)

Thus $\{C_1\}$ and $\{C_2\}$ can be generated by multiplying the $|B|$ matrix by the pressure intensity at the two ends. Assuming that the distribution along the segment is not radically different from functions used to generate the $|B|$ matrix, these load vectors will be reasonably accurate. In the eigenvalue problem, the pressures are functions of the displacements and mass. Since the displacements must be continuous and smooth, then the pressures will be well behaved and the above approximation is very good.

$$\{C_1\} = |B_1| \{p_1\} + |B_2| \{p_2\}$$

$$\{C_2\} = |B_3| \{p_1\} + |B_4| \{p_2\}$$

where $\{p_1\} = \rho\omega^2 h \begin{bmatrix} W_1 \\ U_{\phi 1} \\ \beta_{\phi 1} \\ U_{\theta 1} \end{bmatrix}$, etc.

where ρ = mass density

h = thickness

ω = circular frequency

The iterative procedure follows the cycle.

1. Take the last calculated deflections as assumed deflections for next try (to start with, assume $W = 1$, $U_\phi = \beta_\phi = U_\theta = 0$, everywhere).

2. Calculate load vector for each segment, $\{C\} = \rho h [B] \{U_i\}$

3. Solve for new displacements, $\{U_{i+1}\}$

4. Scale new displacements so that largest value is one.

5. Compare new displacements with assumed displacements; stop if

$$\sum_{j=1}^{M} \left| U_{j,i+1} - U_{j,i} \right| < \varepsilon M,$$ where ε is error criterion supplied by user and M is total number of displacements; otherwise continue iterating with step 1.

The above procedure converges to the lowest longitudinal mode. In order to find higher modes the lower modes must be swept out during each iteration. The sweeping is done between steps 3 and 4. The lower modes are eliminated by utilizing the well known fact that

$$\{\phi_\ell^T\} |M_n| \{\phi_m\} = 0 \qquad \ell \neq m$$

where ϕ_m = displacement vector of mth mode, etc.

Since $[B_n]$, the assembled influence matrix, is approximately proportional to $|M_n|$, it is used in place of $|M_n|$. If the total number of modes already found is K, then after $\{U_{i+1}\}$ has been obtained in step 3, it is assumed that

$$\{U_{i+1}\} = \{\bar{U}_{i+1}\} + \sum_{m=1}^{K} \alpha_m \{\phi_m\}$$

where $\bar{U}_{i+1}$ = vector which is orthogonal to $\{\phi_m^T B_n\}$, m = 1,K

Premultiplying by $\left\{\phi_m^T\right\}\left[B_n\right]$ yields

$$\alpha_m = \frac{\phi_m^T B\ U_{i+1}}{\phi_m^T B\ \phi_m} \qquad m = 1,K$$

and $\left\{\overline{U}_{i+1}\right\}$ can be determined.

Then $\left\{\overline{U}_{i+1}\right\}$ is scaled in step 4, and the process continues.

5. Direct Time Integration Solutions (Prog. 1374)

The direct time integration subroutine uses the same influence matrix $|B|$ that is used in the eigenvalue subroutine. To determine the accelerations at a given time, Houbolts'* scheme is used

$$\left\{\ddot{U}_i\right\} = 2\left\{U_i\right\} - 5\left\{U_{i-1}\right\} + 4\left\{U_{i-2}\right\} - \left\{U_{i-3}\right\} / \Delta t^2$$

where Δt = time increment

Thus for each segment,

$$\left\{\bar{P}_{1,i}\right\} = \frac{\rho h}{\Delta t^2}\left\{2U_{1,i} - 5\,U_{1,i-1} + 4\,U_{1,i-2} - U_{1,i-3}\right\} + \left\{P_{1,i}\right\}$$

where $\left\{P_{1,i}\right\}$ = applied pressure intensity at end 1 at time t_i

ρh = mass/sq. inch of surface

Then

$$\left|C_1\right| = \left|B_1\right|\left|\bar{P}_{1,i}\right| + \left|B_2\right|\left|\bar{P}_{2,i}\right|$$

$$\left|C_2\right| = \left|B_3\right|\left|\bar{P}_{1,i}\right| + \left|B_4\right|\left|\bar{P}_{2,i}\right|$$

Having obtained the new load vector $|C|$, the displacements and forces at time t_i are solved for in the usual manner.

* See Reference (5)

REFERENCES

(1) A. Kalnins, "Analysis of Shells of Revolution Subjected to Symmetrical and Non-Symmetrical Loads", Trans. of the ASME, Journal of Applied Mechanics, Sept. 1964, pp 467-476.

(2) H. Kraus, Thin Elastic Shells, John Wiley & Sons, Inc., New York, 1967. pp 419-430

(3) A. Kalnins, "On Free and Forced Vibration of Rotationally Symmetric Layered Shells", Trans. of the ASME, Journal of Applied Mechanics, Dec. 1965, pp. 941-943.

(4) W. C. Hurty & M. F. Rubenstein, Dynamics of Structures Prentice-Hall Book Company, Inc., Englewood Cliffs, New Jersey, 1964.

(5) J. C. Houbolt, "A Recurrence Matrix Solution for the Dynamic Response of Elastic Aircraft", J. Aero Sci..17, 1950, pp 540-550.

CBI

PROGRAM E0781A

The Shells of Revolution Program is the Chicago Bridge & Iron Company Program E0781A. The program calculates the stresses and displacements in thin-walled elastic shells of revolution when subjected to static edge, surface and/or temperature loads with arbitrary distribution over the surface of the shell. The geometry of the shell must be symmetric, but the shape of the median is arbitrary. It is possible to include up to three branch shells with the main shell in a single model. In addition, the shell wall may consist of four layers of different orthotropic materials, and the thickness of each layer and the elastic properties of each layer may vary along the median.

Program E0781A numerically integrates the eight ordinary first order differential equations of thin shell theory derived by H. Reissner. The equation are derived so that the eight variables which appear on the boundaries of the axially symmetric shell are chosen so that the entire problem can be expressed in these fundamental variables.

Chicago Bridge & Iron Company has extensively revised the Kalnins Program. The program has been altered so that a 4 x 4 force-displacement relation can be used as a boundary condition as an alternative to the usual procedures of specifying forces or displacements. This force-displacement relation can be used to describe the forces at the boundary in terms of displacements at the boundary, or the displacements at the boundary in terms of forces or some compatible combination of the two. In this manner, it is possible to study (RE TYPED)

PROGRAM E0781A

the behavior of a large complex structure. It is also possible to introduce a "spring matrix" at the end of any part of the stress model. This matrix must be expressed in the form, force = spring matrix x displacement. In this manner it is possible to model the restraint of the sand cushion in the transition zone at the point of the embedment. In addition to the above changes, the Kalnins Program has been modified to increase the size of the problem that can be considered and to improve the accuracy of the solution.

RE-TYPED

SUBJECT PROGRAM E0781A	MADE BY REA	CHKD BY	1 REV	By DHA	CHARGE NO. 72-4333
DESCRIPTION	DATE 10/9/74	DATE 10/11/74		Chkd WJR Date 11-6-77	CB-16 SHT ____ OF ____

PROGRAM 781

METHOD OF MODELING VERTICAL STIFFENERS

N = No. of vertical stiffeners around

E = Modulus of elasticity

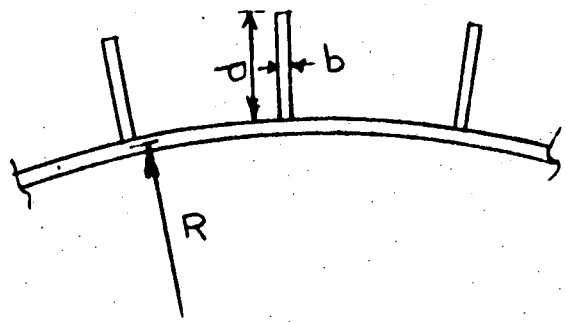

FIG. 1

The shell shown in Fig. 1 is modeled using 2 layers. The inside layer represents the shell and, therefore, has the normal isotropic material properties. The outer layer, on the other hand, is described as an orthotropic material having the following properties.

$$t_2 = d$$

$$E\phi_2 = \frac{bN}{2\pi R} E$$

$$E\theta_2 = 0$$

$$G\phi\theta_2 = 0$$

where

t_2 = Thickness of outer layer

$E\phi_2$ = Modulus of elasticity of outer layer in longitudinal direction

$E\theta_2$ = Modulus of elasticity of outer layer in circumferential direction.

$G\phi\theta_2$ = Shear modulus of outer layer.

PROGRAM 1017

Modal Analysis of Structures Using the Eigenvalue Technique

The purpose of this program is three-fold:

1. To calculate the mass and stiffness matrices associated with the structural model.
2. To determine the undamped natural periods of the model.
3. To calculate the maximum modal responses of the structure i.e. deflections, shears, and moments.

The stiffness and mass matrices may be required in order to perform a dynamic analysis of the structure. The maximum modal responses may be used to perform a spectral analysis.

The program has the following options:

1. Vertical translation.
2. Torsional modes.
3. Soil-structure interaction.
4. Liquid sloshing.
5. Direct introduction of stiffness and mass matrices.

Solution of the Problem

The equations of motion describing the lumped mass system having n degrees of freedom are

$$[M]\{\ddot{X}\} + [C]\{\dot{X}\} + [K]\{X\} = \{P\} \qquad (1)$$

where

$[M]$ = the mass matrix (n x n)

$[C]$ = the damping matrix (n x n)

$[K]$ = the stiffness matrix (n x n)

It has been shown that for certain types of damping or, for moderate amounts of damping, the maximum response can be obtained from a study of the free vibrations of the structure[1]

$$[M]\{\ddot{X}\} + [K]\{X\} = \{0\} \qquad (2)$$

Assume

$$\{X\} = \{\phi\} \sin wt$$

Thus

$$\{-w^2 [M] + [K]\}\{\phi\} = \{0\} \qquad (3)$$

and for a solution to exist

$$|-w^2 [M] + [K]| = 0 \qquad (4)$$

Expanding the determinant given in (4) and solving the resulting equation yields solutions for w^2. These solutions are the eigenvalues of the system. The periods of the structure are obtained using the following relationship

$$T_i = \frac{2\pi}{w_i} \qquad i = 1,n$$

Hence, a n degree of freedom structure has n natural periods of vibration.

After the eigenvalues are obtained, the maximum displacements for each mode are calculated using equation (3). Since the solution of these equations is not unique, all of the mass point displacements must be determined in relation to each other. This is done for all of the modes, yielding n deflection patterns. Note that all of the displacements in any individual mode have the correct relationship to each other while there is as yet no relationship between the magnitudes of the various mode shapes.

The n x n matrix having the displacements for each mode shape contained in its columns is called the eigenvector array (ϕ).

In order to relate the mode shapes to each other, it is necessary to calculate a participation factor for each mode.

The undamped equation of motion is

$$[M]\,\{\ddot{X}_i\} + [K]\,\{X_i\} = \{P_i\} \tag{5}$$

Assume that

$$\{X_i\} = [\phi_{im}]\,\{u_m\} \qquad i = 1,2,3,\ldots,n \tag{6}$$

m = mode number

Substituting (6) into (5) and also premultiplying each side by $[\phi_{im}]^T$ yields[2]

$$[\cancel{M_m}]\,\{\ddot{u}_m\} + [\cancel{K_m}]\,\{u_m\} = \{P_m\} \tag{7}$$

where

$$[M_m] = [\phi_{im}]^T\,[M]\,[\phi_{im}] \tag{7a}$$

$$[\cancel{K_m}] = [\phi_{im}]^T\,[K]\,[\phi_{im}] \tag{7b}$$

$$P_m = [\phi_{im}]^T\,P_i \tag{7c}$$

Thus, we now have n uncoupled equations of the form

$$M_m\ddot{u}_m + K_m u_m = P_m$$

or

$$\ddot{u}_m + w^2_m u_m = \frac{P_m}{M_m} \tag{8}$$

For earthquake loading

$$|P_i| = -|m_i| \ddot{u}g \tag{9}$$

$\ddot{u}g$ = earthquake acceleration

$|m_i|$ = column mass matrix consisting of mass terms which would be multiplied by incident acceleration if forced vibrations were being considered.

The general solution of eqn (8) i.e. the response of the mth mode is given by the Duhamel Integral

$$u_m(t) = \int_0^t \frac{P_m}{M_m w_m} \sin w_m (t-\tau) d\tau \tag{10}$$

Substituting (9) into (10) and using (7c) yields

$$u_m = u_m(t) = -\frac{|\phi_{im}|^T |m_i|}{M_m w_m} \int_0^t \ddot{u}g(\tau) \sin w_m (t-\tau) d\tau \tag{11}$$

Now

$$S_{am} = [w_m \int_0^t \ddot{u}g(\tau) \sin w_m (t-\tau) d\tau]max \tag{12}$$

where S_{am} is the spectral acceleration for the period associated with the mth mode.

Substituting (12) into (11)

$$(u_m)_{max} = -\frac{|\phi_{im}|^T |m_i|}{M_m w_m^2} S_{am} \tag{13}$$

Since $S_{Dm} = S_{am}/w^2$ where S_{Dm} is the spectral displacement

$$(u_m)_{max} = \frac{|\phi_{im}|^T |m_i|}{M_m} S_{Dm} \tag{14}$$

Using (7a) and (14) yields

$$(u_m)_{max} = -\frac{|\phi_{im}|^T |m_i|}{|\phi_{im}|^T [m_i] |\phi_{im}|} S_{Dm} \tag{15}$$

Therefore, eqn (15) yields the "participation" or "scale" factor γ_m for each mode.

$$\gamma_m = \frac{|\phi_{im}|^T |m_i|}{|\phi_{im}|^T [m_i] |\phi_{im}|} \tag{16}$$

Assuming α_m is the desired maximum response for a particular mode.

$$a_m = \gamma_m \alpha\phi_m S_{Dm}$$

where $\alpha\phi_m$ is the response based upon the eigenvectors of the mode obtained by eqn (3).

The next step that is necessary is to obtain the maximum total response by combining the responses of the various modes. Since only rarely do all the modal responses obtain their maximum at the same time, some judgment must be exercised. An envelope of maximum response can be obtained by direct addition of all of the modal responses. However, in some cases, especially when there are a large number of degrees of freedom this method may be grossly conservative. A more accurate method would probably be by combining the modal responses by the "square root of the sum of the squares" method.

As a check on the solution for the eigenvectors, the dot product of the eigenvectors weighted with the mass matrix are calculated by the program.

$$\cos\beta = \frac{\left\{\phi_r\right\}^T [M] \left\{\phi_s\right\}}{\left|\left\{\phi_r\right\}^T [M] \left\{\phi_s\right\}\right|} \qquad r \neq s \qquad (17)$$

It can be shown that the eigenvectors are orthogonal and therefore[2]

$$\cos\beta = 0$$

References

1. Blume, Newmark, & Corning, Design of Multistory Reinforced Concrete Buildings for Earthquake Motions, Portland Cement Association, 1961.

2. Hurty & Rubinstein, Dynamics of Structures, Prentice Hall, 1964.

Note:

An option has been added to the program to obtain the maximum total response. This is done by direct addition of the contribution of each mode the user wants to consider. (See input data cards 14 and 15).

CBI

PROGRAM 1044

SEISMIC ANALYSIS OF VESSEL APPENDAGES

Appendages to a vessel may not significantly contribute structurally to the dynamic responses of a model of a vessel. However, appendages can affect the vessel locally by vibrating differently from the model of the vessel at the point of attachment.

The response spectrum method of analysis is not a strictly adequate way of obtaining the maximum appendage accelerations since it does not include the possible consequences of near resonance between the vessel model and the appendage model.

This paper describes the method used to evaluate the maximum elastic differential accelerations between an independently vibrating appendage model and an elastic beam vessel model at the appendage elevation due to known excitations of the elastic beam model.

The method involves two distinct steps. Firstly, the necessary time-absolute acceleration records are computed at appendage elevations due to model excitations. Secondly, the maximum differential accelerations between each appendage model and the vessel model at the appendage elevation are obtained.

The time-absolute acceleration records at the appendage elevation are computed by use of a step-by-step matrix analysis procedure. The equations of motion for the vessel model are of the form:

$$[M]\{\ddot{u}\} + (AT/\pi)[K]\{\dot{u}\} + [K]\{u\} = -[M]\{\ddot{u}_g\}$$

where

[M] = Mass matrix, order n x n, obtained from a modal analysis.

[K] = Stiffness matrix, order n x n, obtained from a modal analysis.

A = Portion of first mode critical damping for the model.

T = First mode period of the model.

[M] = A diagonal matrix, order n x n, with diagonal elements corresponding to elements of the mass matrix excited by translational accelerations.

$\{\ddot{u}\}$ = n x 1 matrix of relative accelerations between the model base and the n degress of freedom.

$\{\dot{u}\}$ = n x 1 matrix of velocities corresponding to $\{\ddot{u}\}$.

$\{u\}$ = n x 1 matrix of displacements corresponding to $\{\ddot{u}\}$.

$\{\ddot{u}_g\}$ = n x 1 matrix of translation base acceleration.

n = Degrees of freedom of vessel model.

By taking a small time increment (smaller than the smallest period obtained from the modal analysis) and letting accelerations vary linearly within the selected increment, the equations of motion can be integrated for the quantities $|u|$, $|\dot{u}|$, and $|\ddot{u}|$ over the selected time increment.[1] The values obtained are superimposed upon the values of these quantities existing at the beginning of the time increment. This process is repeated for the duration of the excitation. The time-absolute acceleration records for each translational degree of freedom are the sums of $|\ddot{u}|$ and $|\ddot{u}_g|$ taken throughout the history of the excitation.

The second step is similar to the first step. The equation of motion (n = 1) is written for the appendage as a single degree-of-freedom elastic model using the time-absolute acceleration record obtained in step 1 at the appendage elevation as the excitation. This equation is solved in the same manner used in step 1. The maximum absolute value of $|\ddot{u}|$ obtained is the quantity desired. It is the maximum differential acceleration between the appendage model and the vessel model due to a known excitation of the vessel model.

For any appendage, this two-step procedure should be executed three times. This is required to evaluate normal, tangential and vertical appendage accelerations with respect to a vessel cross-section.

[1] Wilson & Clough, Dynamic Response by Step-By-Step Matrix Analysis

PROGRAM E1622

LOAD GENERATION PREPROCESSOR FOR PROGRAM E1374

In order to perform non-axisymmetric analyses on shells, the load must often be defined using Fourier series representation. The purpose of Prog. E1622 is to calculate and store on magnetic tape a time history of the Fourier pressure amplitudes. The format of this tape is designed specifically for use with Program E1374.

The input consists primarily of pressure versus angle versus time data at user supplied elevations. An option of the program enables the TVA furnished data cards for the Watts Bar Containment to be used directly. The pressures given on these cards can be scaled by a factor input by the user.

The program plots the unscaled input pressure versus time for each shell compartment.

In order to calculate the amplitudes of the harmonics, a linear function in the circumferential direction is assumed between given points. (See Figure 1).

The output for user specified time steps will be written on a labeled tape or disk file assigned by the user. Printed output consists of the Fourier amplitudes at every time step plus the total number of timesteps for each harmonic.

Other features and assumptions of the program are:

1. Only distributed loads are considered.

2. The model consists of a cylindrical shell and optional hemispherical top head.

3. The pressure has a block type distribution in the longitudinal direction. (See Fig. 1)

4. Any initial pressure acting on the shell can be subtracted from the input pressure histories.

5. Amplitudes for both sine and cosine terms can be calculated with the user supplying the range of harmonics to be output.

Location

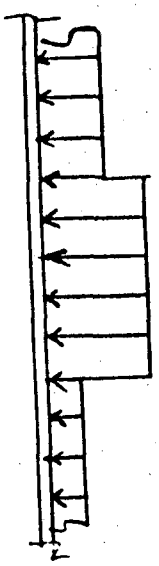

ASSUMED SHAPE OF PRESSURE DISTRIBUTION IN LONGITUDINAL DIRECTION

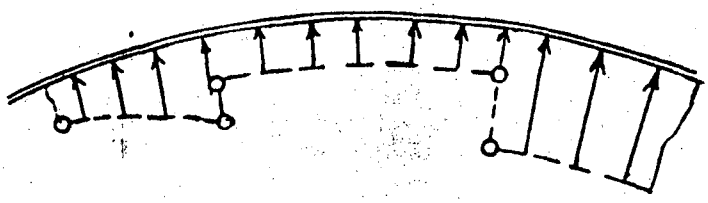

ASSUMED SHAPE IN CIRCUMFERENTIAL DIRECTION

o GIVEN POINTS

--- GENERATED BY PROGRAM E16

$$p(x,\theta,t) = \sum_{n=0}^{m} p_n(x,t)\cos n\theta + \sum_{j=1}^{m} p_j(x,t)\sin j\theta$$

where

$$p_0(x,t) = \frac{1}{2\pi}\int_0^{2\pi} p(x,\theta,t)\,d\theta$$

$$p_n(x,t) = \frac{1}{\pi}\int_0^{2\pi} p(x,\theta,t)\cos n\theta\,d\theta \qquad n \geq 1$$

$$p_j(x,t) = \frac{1}{\pi}\int_0^{2\pi} p(x,\theta,t)\sin j\theta\,d\theta \qquad n \geq 1$$

x = LONGITUDINAL COORDINATE.

θ = AZIMUTH

t = TIME

m = TOTAL NUMBER OF CIRCUMFERENTIAL WAVES

SUBJECT	MADE BY	CHKD BY	REV	By		CHARGE NO.
PROGRAM E1622	CAP	WM		Chkd		72-4333
FIG 1	DATE 10/5/72	DATE 10/11/77		Date		SHT CB20 OF

PROGRAM E1623

POST-PROCESSOR PROGRAM FOR PROGRAM E1374

Program E1623 was written specifically for the TVA Watts Bar Containment Vessels. It performs the following operations:

1. Using Fourier data generated by Program E1374 (Dynamic Shell Analysis), the summed displacements, forces and stresses found for various points around the shell circumference at each output point on the meridian.

2. The maximum of the summed values along with the associated time and azimuth are saved for each elevation and printed out at the end of the problem.

3. The following tables are printed:
   1. Radial deflection w at each elevation versus azimuth
   2. Longitudinal force $N\phi$ at each elevation versus azimuth
   3. Longitudinal moment $M\phi$ at each elevation versus azimuth
   4. Circumferential force $N_{\phi\theta}$ at each elevation versus azimuth

The time basis for these tables is the occurrence of the minimum longitudinal force at the base.

4. Ring forces are calculated using the equations shown in this writeup and then the maximums are pointed out.

5. Displacement traces at several elevations can be saved on a tape or disk unit.

6. The membrane stress resultants are saved on either a tape or disk unit for input into the buckling check program.

Program E1374 writes the Fourier amplitude results of the fundamental variables (w, u_ϕ, β_ϕ, u_θ, Q, $N\phi$, $M\phi$, N) on a labeled tape after each timestep. Program E1623 reads this tape, interpolates to obtain the values at the output times, and calculates the remaining forces[1] and all the stresses.

The amplitudes are then summed using the following equation:

$$f(x,\theta,t) = \sum_{n=0}^{m} g(x,t)\mathrm{Cos}n\theta + \sum_{n=1}^{m} h_n(x,t)\mathrm{Sin}m\theta$$

x = meridianal coordinate

t = time

$g_n(x,t)$ = amplitudes of cosine harmonics

$h_n(x,t)$ = amplitudes of sine harmonics

θ = azimuth

$f(x,\theta,t)$ = Fourier sum

m = maximum number of circumferential waves

CALCULATION OF RING LOADS

The assumptions used are:

1. One of the principal axes of the ring is parallel to the axis of rotation.
2. The ring is symmetric with respect to the principal axis which is perpendicular to the axis of rotation.
3. The shear center is at the centroid.

[1] See p# 472 of Ref. (1) for the equations used.

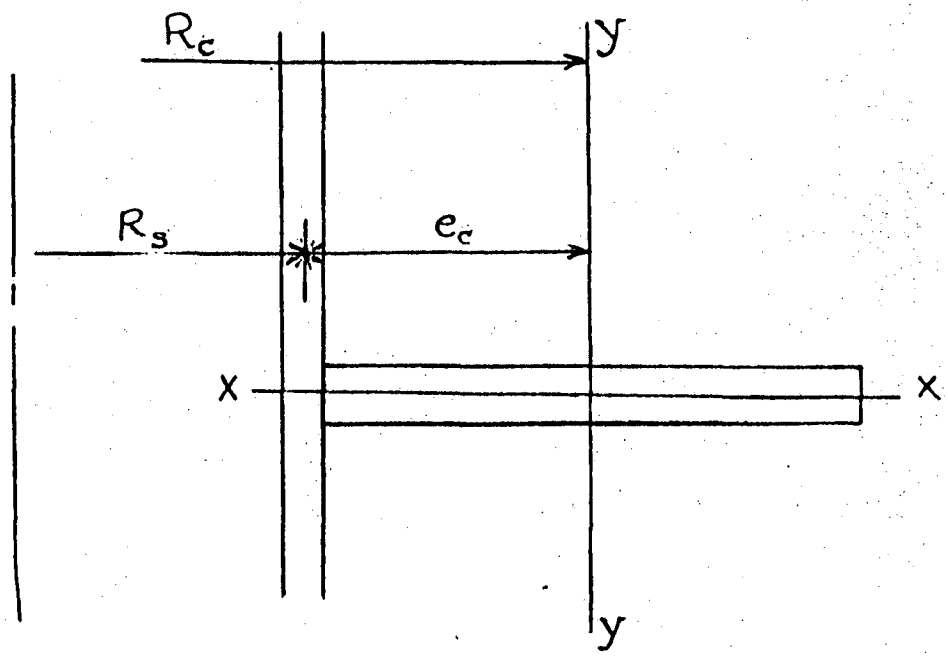

W_r = radial displacement of ring

V_r = tangential displacement of ring

N_θ = circumferential force in ring

M_θ = circumferential moment in ring

E = modulus of elasticity of ring

A = area of ring

I = moment of inertia of ring about y y

W_s = radial displacement of shell

V_s = tangential displacement of shell

$$V_r = V_s\left(1 + e_c/r_c\right) - e_c/r_c\dot{W}$$

$$W_r = W_s$$

$$N_\theta = \frac{EA}{r_c}\left(\dot{V}_r + W_r\right)$$

$$M_\theta = \frac{EI}{r_c^2}\left(-\ddot{W}_r + \dot{V}_r\right)$$

Where a dot denotes differentiation with respect to the circumferential coordinate.

Weld shear - the weld shear equals the jump in shell in-plane shear at the ring.

PROGRAM E1624

SPCGEN - Spectral Curve Generation

Program E1624 reads the Fourier amplitudes of the deflection transients stored on magnetic tape from the output of program E1374. The program then proceeds as follows to calculate the accelerations at uniform time intervals and to evaluate the response spectra:

1. From the deflection transient for each harmonic, the acceleration traces are computed using three point central difference for the first and last three time steps, and a seven point central difference elsewhere.

   a. Three point central difference equation:
   let $y = f(t)$ be the function that fits a data set, then a three point central difference equation is:

$$\left(\frac{d^2y}{dt^2}\right)_i = \frac{1}{h^2}\left(y_{i+1} - 2y_i + y_{i-1}\right)$$

   where,
   $y_{i+1} = f(t_{i+1})$, $y_i = f(t_i)$, and $y_{i-1} = f(t_{i-1})$

   are three consecutive displacements in the data set at equal time intervals h, where $h = t_{i+1} - t_i = t_i - t_{i-1}$

   b. Seven point central difference equation:
   The seven point central difference equation, using Stirling's formula at $t = t_i$, is:

$$\left(\frac{d^2y}{dt^2}\right)_i = \frac{1}{180h^2}\Big[\,2\left(y_{i+3} + y_{i-3}\right) - 27\left(y_{i+2} + y_{i-2}\right) + 270\left(y_{i+1} + y_{i-1}\right) - 490y_i\,\Big]$$

where, $y_{i+3} = f\left(t_{i+3}\right)$, $y_{i+2} = f\left(t_{i+2}\right)$, etc....

and h is as defined above.

2. The Fourier amplitudes of the acceleration transient for each harmonic obtained in step 1 are interpolated to obtain a common timestep.

3. The accelerations of step 2 are summed for given angles:

$$\left(\frac{d^2y}{dt^2}\right)_{@\theta} = \sum_{n=1}^{n=k} A_n \sin n\theta + \sum_{n=0}^{n=j} B_n \cos n\theta$$

where,

n = number of circumferential waves (harmonic number)

k = number of sine harmonics

j = number of cosine harmonics

4. CBI program E1668 is now used as a subroutine to evaluate the dynamic response spectra and present the results on printed plots. A brief description of this program follows.

Description of Program E13910

Shell Buckling Analysis for TVA Containment Vessel

Introduction

Program #13910 performs the buckling check of the TVA ice condenser containment vessel for Non-axisymmetric pressure loading combining with the dead loads and seismic loads occuring in the vessel. The non-axisymmetric loads are developed by CBI program E1374. The resulting stresses are compared to critical buckling stress and by using a specified factor of safety the buckling ratio is found.

Calculation of Dead Loads and Seismic Loads

As a general rule, dead loads and seismic loads are calculated at a few points along the vessel and the vessel is checked for buckling at many more points. As a result the program performs a linear interpolation to derive the dead loads and seismic loads at any given point along the vessel.

Calculation of Critical Buckling Stresses

In order to determine the critical buckling stress at a given point it is necessary to determine the geometry in the region of that point. The program considers four cases:

a) cylinders stiffened meridionally and circumferentially
b) cylinders stiffened circumferentially
c) spheres stiffened circumferentially and meridionally
d) unstiffened spheres

For each of these conditions certain constants must be determined based on known geometry. This information is in the form of graphs and is input into the computer as a series of straight lines. Once these constants are known, the critical buckling stresses can be determined using the applicable formulae. These calculations are based on Appendix H of TVA specification 1440.

Calculation of Stress and Buckling Ratios

The program calculates stresses and buckling ratios at any number of elevations and azimuths and for any number of time periods and then finds the maximum buckling ratio at each elevation. The program calculates four stresses at each point:

a) meridional stress due to axial loads
b) meridional stress due to bending loads
c) circumferential stress
d) shear stress

The program considers only compressive stresses. If a stress is tensile it is set equal to zero. For each of the stresses a buckling ratio is calculated using the stress multiplied by a factor of safety and divided by the critical buckling stress. These buckling ratios are then combined and five ratios result:

a) Axial + Circumferential
b) Axial + Bending
c) Axial + Shear
d) Axial + Shear + Bending
e) Axial + Shear + Circumferential

After these combined ratios are calculated, the maximums regardless of time or azimuth are recorded for each elevation.

In areas where vertical stiffening is present the program calculates the buckling ratio of the stiffener acting with the shell as a column simply supported at each end. The portion of the shell used in the column is determined using the rules of the Shell Analysis Manual referenced in Appendix H of Specification 1440. The buckling ratio is calculated in the manner discussed previously and the maximum is recorded.

Program Output

The program prints out the following data at each elevation considered:

a) Basic shell data and geometry of stiffeners
b) Load such as static pressure, dead loads, and seismic loads
c) Buckling stress coefficient
d) The five combined buckling ratios.
e) Vertical stiffener buckling ratios

PROGRAM E1668

SPECTR - Spectral Analysis for Acceleration Records Digitized at Equal Intervals

Program E1668 evaluates dynamic response spectra at various periods and presents the results on a printed plot. Given the time-acceleration record, the program numerically integrates the normal convolution time integral for various natural periods and damping ratios. The computed relative displacements, relative and pseudo-relative velocities, and absolute and pseudo-absolute accelerations are tabulated for periods from 0.025 seconds to 1 second.

Mathematical Formulation

For a single degree of freedom system, the equation of motion is

$$m\ddot{x} + c\dot{x} + kx = -m\ddot{s}(t) \tag{1}$$

where m, c, and k are the mass, damping, and stiffness, respectively.

Dividing by m, the following equation is obtained.

$$\ddot{x} + 2\beta\,\omega\dot{x} + \omega^2 x = -\ddot{s}(t) \tag{2}$$

β = percentage of critical damping

ω = circular frequency

the solution of Eq. (2) is

$$x(t) = c(t) - \Lambda(t) \tag{3}$$

where

$$c(t) = e^{-\beta\omega t}\left(\frac{\dot{x}_o + \beta\omega x_o}{\bar{\omega}} \sin(\bar{\omega}t) + x_o \cos(\bar{\omega}t)\right)$$

$$A(t) = \int_o^t \frac{1}{\bar{\omega}} e^{-\beta\omega(t-\tau)} \ddot{s}(\tau) \sin\left[\bar{\omega}(t-\tau)\right] d\tau$$

$$\bar{\omega} = \omega \quad (1-\beta^2)$$

$\dot{x}_o$ and x_o are the initial velocity and displacement respectively.

At any point in time during the acceleration trace, c(t) is re-evaluated such that the initial conditions are assumed to be the velocity and displacement obtained at the previous step. Thus, the integration for A(t) needs to be performed over only one timestep interval.

The relative velocity at each time is obtained by differentiating Eq. (3). Then Eq. (2) can be employed to determine the absolute acceleration.

The spectral values are then defined as the maximum values of x, $\dot{x}$, and $\ddot{x}$, occurring during the record. The pseudo-relative velocity and pseudo-absolute acceleration are then calculated using the following equations.

$$v = \omega x_{max}$$

$$a = \omega^2 x_{max}$$

SHELL DESIGN

The Containment Vessel is designed for static internal pressure loading in accordance with the ASME Boiler and Pressure Vessel Code, Section III, Nuclear Power Plant Components and Section VIII, Division 1, Pressure Vessels with Winter 1971 Addenda. The shell formulae used in determining the minimum required shell thicknesses are from Paragraph UG-27 of Section VIII and are shown below:

Circumferential Direction (Cylindrical Vessel)

$$t = \frac{PR}{SE - 0.6P}$$

Meridional Direction (Cylindrical Vessel)

$$t = \frac{PR}{2SE + 0.4P}$$

Spherical Shell

$$t = \frac{PR}{2SE - 0.2P}$$

where: t = minimum required shell thickness (inches)

P = internal pressure (psi)

R = vessel radius (inches)

S = Allowable Stress Value (psi)

E = Shell joint weld efficiency

Other portions of the Containment Vessel such as the penetrations and the personnel lock barrel are designed in accordance with the above rules as applicable.

The Containment Vessel shell and stiffener rings are designed in accordance with Paragraph UG-28 of Section VIII for external pressure.

The containment vessel is designed and analyzed for the non-axisymmetric pressure transient loads resulting from a loss-of-coolant accident in accordance with TVA Specification 1440. Stresses are limited to the allowable stress values stated in Section A of this Stress Report. In addition. a buckling analysis is performed to determine the stability of the vessel in accordance with Appendix H, Revision 1, of TVA Specification 1440. which is reprinted at the end of this section.

PENETRATIONS

The penetrations and reinforcement are proportioned in accordance with the rules presented in Paragraph NE-3330 of Section III. In addition, the penetration assemblies and surrounding shell of loaded penetrations are designed and analyzed in accordance with the rules presented in the Welding Research Council Bulletin Number 107. Permanent caps for spare penetrations are designed in accordance with Paragraph UG-34 of Section VIII. The flanges and bolted covers are designed in accordance with Appendix II of Section VIII.

ATTACHMENTS

Attachments to the Containment Vessel pressure boundary or to material required for the pressure retaining function are designed in accordance with the ASME Code, and the stresses are limited to that allowed by the ASME Code. These rules are applied to the attachment for a distance from the pressure retaining material of 16 times the attachment thickness or 4 inches, whichever is lesser. The remainder of the attachment and other items covered by this Stress Report are designed in accordance with the rules of the AISC Manual of Steel Construction, Seventh Edition.

BOTTOM LINER

Although the bottom liner is furnished by CBI, the design responsibility is by TVA. The rules of Section III of the ASME Code are not applicable.

CBI

GENERAL REFERENCES

1. ASME Boiler and Pressure Vessel Code, 1971 Edition with Winter 1971 Addenda, including the following sections:

   a) Section II, Material Specifications

   b) Section III, Nuclear Power Plant Components

   c) Section VIII, Division 1, Pressure Vessels

2. Manual of Steel Construction, American Institute of Steel Construction, Seventh Edition.

3. John F. Harvey, Pressure Vessel Design, Van Nostrand, Princeton, New Jersey, 1963.

4. S. Timoshenko and S. Woinowsky - Krieger, Theory of Plates and Shells, McGraw-Hill, New York, Second Edition, 1959.

5. W. Flugge, Stresses in Shells, Springer-Verlag, Berlin, Germany, 1962.

6. S. Timoshenko, Theory of Elastic Stability", Engineering Societies Monograph, McGraw-Hill, New York, 1936.

7. O. Blodgett, Design of Welded Structures, The James F. Lincoln Arc Welding Foundation, Cleveland, Ohio, 1966.

8. K. R. Wichman, et.al, "Local Stresses in Spherical and Cylindrical Shells due to External Loadings", Welding Research Council, Bulletin Number 107, August, 1965.

9. Raymond J. Roark, Formulas For Stress and Strain, McGraw-Hill, New York, Fourth Edition, 1965.

10. E. M. Baker, et.al, Shell Analysis Manual, National Aeronautics and Space Administration, Washington, D.C., April, 1968.

11. A. Kalnins, "Analysis of Shells of Revolution Subjected to Symmetric and Non-Symmetric Loads", Transactions of the ASME Journal of Applied Mechanics, September, 1964.

12. M. Kraus, Thin Elastic Shells, John Wiley, New York, 1967.

13. A. Kalnins, "On Free and Forced Vibration of Rotationally Symmetric Layered Shells", Transactions of the ASME, Journal of Applied Mechanics, December, 1965.

14. W. C. Hurty and M. F. Rubenstein, Dynamics of Structures, Prentice-Hall, Englewood Cliffs, New Jersey, 1964.

15. J. C. Houbolt, "A Recurrence Matrix Solution For The Dynamic Response of Elastic Aircraft," J. Aero. Sci. 17, 1950.

16. L. E. Grinter Theory of Modern Steel Structures, Volume II, Macmillan, New York, 1949.

CBI

Location BIRMINGHAM DESIGN

Subsection CE

Computer Programs Used by Anamet

SUBJECT	MADE BY	CHKD BY	REV	By		CHARGE NO.
ANAMET COMPUTER	REA					72-4333
PROGRAMS	DATE 11-5-74	DATE		Chkd		CE-0
				Date		SHT ____ OF ____

GO 64 REV 4-73

Anamet Lab. #1272.230
December 23, 1972
Revised October 31, 1973

PROGRAM BALL
ANALYSIS OF NONLINEAR DYNAMIC SHELLS OF REVOLUTION

By

R. L. Citerley
R. E. Ball

Anamet Laboratories, Inc.
727 Industrial Road
San Carlos, California 94070

CE-1

Anamet Laboratories, Inc.

P.O. BOX 831, SAN CARLOS, CALIFORNIA 94070

TABLE OF CONTENTS

I INTRODUCTION 1

II THEORY

A. Shell Geometry 2
B. Strain-displacement Relations 4
C. Equations of Motion 6
D. Constituitive Relations 7
E. Boundary Conditions 9
F. Ring Stiffeners 10

III METHOD OF SOLUTION

A. Fourier Expansions 14
B. Modal Uncoupling 14
C. Spatial Finite Difference Formulation . 16
D. Time-Wise Differencing. 19
E. Damping 22
F. Solution by Elimination 22
G. Poles 24
H. Computer Program 25

IV REFERENCES 27

APPENDIX A - ELASTIC STATIC

APPENDIX B - BIFURCATION STATIC

APPENDIX C - NONLINEAR DYNAMIC

APPENDIX D - ELASTIC WITH RINGS-STATIC

APPENDIX E - ELASTIC ORTHOTROPIC DYNAMIC

APPENDIX F - FULL FOURIER EXPANSIONS

Anamet Laboratories, Inc.

P.O. BOX 831, SAN CARLOS, CALIFORNIA 94070

I INTRODUCTION

The numerical analysis of thin shells of revolution is a subject that has received a considerable amount of attention in recent years. Most of this attention has been given to the linear analysis of symmetric and nonsymmetric loaded shells. The dynamic (transient) behavior of shells has also been given some attention. Little discussion has been presented for the static nonlinear behavior of a shell of revolution. Further, discussions on the nonlinear transient behavior of nonsymmetrically loaded shells are minimal.

Anamet and its consultants have illustrated the nonlinear dynamic behavior of isotropic shells of revolution.[1,2,3,4*] The purpose of this study is to report upon a nonlinear, dynamic shell of revolution computer program which permits the inclusion of circumferential rings. Sanders[5] nonlinear equations of equilibrium are used as the basis of this development. The constituitive relations used by Sanders are the same as Love's first approximation. A compatible set of equilibrium equations is derived for discrete circumferential rings and layered orthotropic shells. Program efficiency is attained by the described variable mesh spacing. The above features are provided in the BALL computer program. Even though the development is based upon a nonlinear theory, this program is applicable to linear, elastic, dynamic behavior of shells of revolution. The linear and nonlinear features of the BALL program are illustrated by a number of sample solutions. These results are compared to other published results.

* superscript numbers denote references.

CE-3

II THEORY

A. Shell Geometry

Consider the general shell of revolution shown in figure 1. Located within this shell is a reference surface. All material points of the shell can be located using the orthogonal coordinate system s, θ, ζ, where s is the meridional distance along the reference surface measured from one boundary, θ is the circumferential angle measured from a datum meridian plane, and ζ is the normal distance from the reference surface. Further, let the location of the reference surface be described by the dependent variable r, the normal distance from the axis of the shell. Accordingly, the principal radii of curvature of the reference surface are

$$R_\theta = r/[1 - (r')^2]^{\frac{1}{2}} \tag{1}$$

$$R_s = - [1 - (r')^2]^{\frac{1}{2}}/r'' \tag{2}$$

where a prime denotes differentiation with respect to s. Further, note the Codazzi identity

$$\left(\frac{1}{R_\theta}\right)' = r' \left(R_s^{-1} - R_\theta^{-1}\right)/r \tag{3}$$

and the relation

$$r'' = - r/R_s R_\theta \tag{4}$$

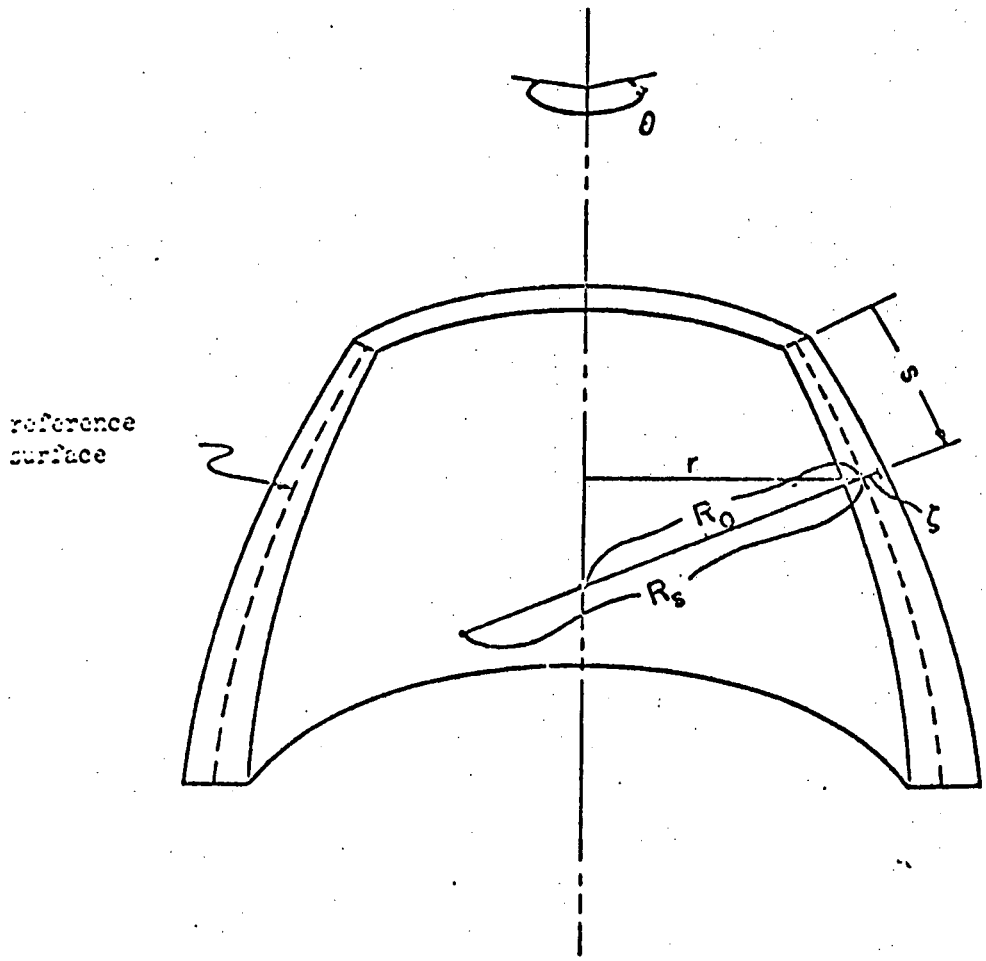

Figure 1. Shell Geometry and Coordinates

CE-5

B. Strain-displacement Relations

For a shell of revolution, the strain-displacement relations derived by Sanders[5] take the form

$$\left.\begin{aligned} \varepsilon_s &= U' + W/R_s + (\phi_s^2 + \phi^2)/2 \\ \varepsilon_\theta &= \dot{V}/r + r' U/r + W/R_\theta + (\phi_\theta^2 + \phi^2)/2 \\ \varepsilon_{s\theta} &= (V' + \dot{U}/r - r'V/r + \phi_s \phi_\theta)/2 \end{aligned}\right\} \quad (5)$$

$$\left.\begin{aligned} \kappa_s &= \phi_s' \\ \kappa_\theta &= \dot{\phi}_\theta/r + r' \phi_s/r \\ \kappa_{s\theta} &= [\phi_\theta' + \dot{\phi}_s/r - r' \phi_\theta/r + (R_\theta^{-1} - R_s^{-1}) \phi]/2 \end{aligned}\right\} \quad (6)$$

where ε_s, ε_θ, and $\varepsilon_{s\theta}$ are the reference surface strains, κ_s, κ_θ, and $\kappa_{s\theta}$ are the bending strains, U and V are displacements in the directions tangent to the meridian and to the parallel circle respectively, W is the displacement normal to the reference surface, and ϕ_s, ϕ_θ, and ϕ are rotations defined by

$$\left.\begin{aligned} \phi_s &= - W' + U/R_s \\ \phi_\theta &= - \dot{W}/r + V/R_\theta \\ \phi &= (V' + r'V/r - \dot{U}/r)/2 \end{aligned}\right\} \quad (7)$$

In these equations, and henceforth, a superscript dot denotes differentiation with respect to θ. The positive direction of each displacement and rotation variable is indicated in figure 2.

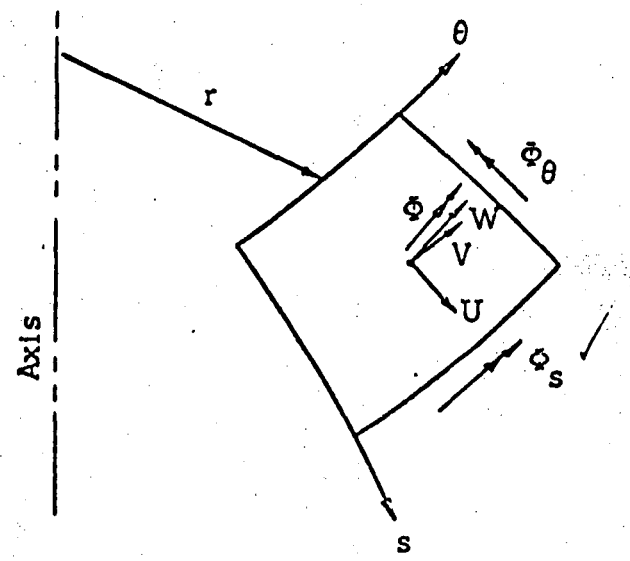

Figure 2. Positive Directions for Displacements and Rotations

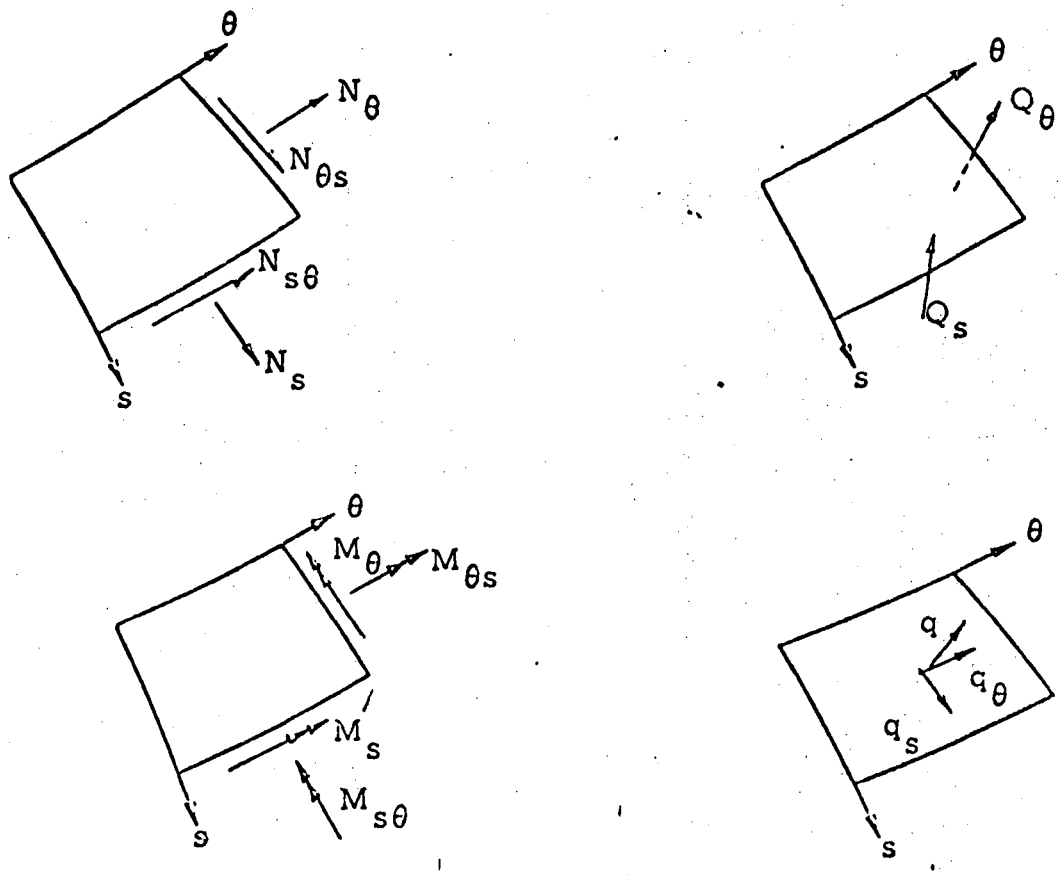

Figure 3. Positive Directions for Forces, Moments and Loads

CE-7

C. Equations of Motion

Converting Sanders' equilibrium equations to the equations of motion for a shell of revolution leads to

$$
\left.
\begin{aligned}
&(rN_s)' + N_{s\theta}^{\bullet} - r'N_\theta + rQ_s/R_s + (R_s^{-1} - R_\theta^{-1})\, M_{s\theta}^{\bullet}/2 = r(\textstyle\int m\,d\zeta)\partial^2 U/\partial T^2 \\
&- rq_s + \underline{r(\Phi_s N_s + \Phi_\theta N_{s\theta})/R_s} + \underline{[\Phi(N_s + N_\theta)]^{\bullet}/2} \\
&N_\theta^{\bullet} + (rN_{s\theta})' + r'N_{s\theta} + rQ_\theta/R_\theta + r[(R_\theta^{-1} - R_s^{-1})M_{s\theta}]'/2 = \\
&r(\textstyle\int m\,d\zeta)\partial^2 V/\partial T^2 - rq_\theta + \underline{r(\Phi_\theta N_\theta + \Phi_s N_{s\theta})/R_\theta} - \underline{r[\Phi(N_s + N_\theta)]'/2} \\
&(rQ_s)' + Q_\theta^{\bullet} - rN_s/R_s - rN_\theta/R_\theta = r(\textstyle\int m\,d\zeta)\partial^2 W/\partial T^2 \\
&- rq + \underline{(r\Phi_s N_s + r\Phi_\theta N_{s\theta})'} + \underline{(\Phi_s N_{s\theta} + \Phi_\theta N_\theta)^{\bullet}}
\end{aligned}
\right\} \quad (8)
$$

*

and

$$(rM_s)' + M_{s\theta}^{\bullet} - r'M_\theta - rQ_s = 0 \qquad (9)$$

$$M_\theta^{\bullet} + (rM_{s\theta})' + r'M_{s\theta} - rQ_\theta = 0 \qquad (10)$$

when the effects of rotary inertia are neglected. In equations (8) - (10), m is the mass density of the shell material, T is time, q_s, q_θ, and q are the meridional, circumferential, and normal components of the applied pressure load, Q_s and Q_θ are the transverse forces per unit length, N_s, N_θ, and $N_{s\theta}$ are the membrane forces per unit length, and M_s, M_θ, and $M_{s\theta}$ are the bending and twisting moments per unit length. Refer to Figure 3 for the positive directions of the pressure components, forces, and moments.

* underlined terms are the nonlinear terms

Andmet Laboratories, Inc.

P.O. BOX 831, SAN CARLOS, CALIFORNIA 94070

D. Constituitive Relations

The constitutive stress-strain-temperature relations assumed for the elastic behavior of the shell along the meridian are the following equations relating the force and moment resultants and strain and curvature expressions.

$$\begin{Bmatrix} N_s \\ N_\theta \\ N_{s\theta} \\ M_s \\ M_\theta \\ M_{s\theta} \end{Bmatrix} = \begin{bmatrix} C_{11} & C_{12} & 0 & K_{11} & K_{12} & 0 \\ C_{12} & C_{22} & 0 & K_{12} & K_{22} & 0 \\ 0 & 0 & C_{33} & 0 & 0 & K_{33} \\ K_{11} & K_{12} & 0 & D_{11} & D_{12} & 0 \\ K_{12} & K_{22} & 0 & D_{12} & D_{22} & 0 \\ 0 & 0 & K_{33} & 0 & 0 & D_{33} \end{bmatrix} \begin{bmatrix} e_s \\ e_\theta \\ e_{s\theta} \\ k_s \\ k_\theta \\ k_{s\theta} \end{bmatrix} + \begin{Bmatrix} C_{1T} \\ C_{2T} \\ 0 \\ D_{1T} \\ D_{2T} \\ 0 \end{Bmatrix} \quad (11)$$

Where

$$C_{ij} = \int B_{ij}\, d\zeta \quad (12a)$$

$$K_{ij} = \int B_{ij}\, \zeta\, d\zeta \quad (12b)$$

$$D_{ij} = \int B_{ij}\, \zeta^2\, d\zeta \quad (12c)$$

$$B_{ij} = \frac{E_{ij}}{1-\nu_i\nu_j} \quad \text{where } i = j = 1,2 \;;\; B_{ij} = \frac{E_{ii}\,\nu_j}{1-\nu_i\,\nu_j}\,,\; i \neq j = 1,2 \quad (12d)$$

$$B_{ij} = 2G_{ij} \qquad \text{where } i, j = 3 \quad (12e)$$

$$C_{iT} = \int \alpha\, \tau\, E\, d\zeta \;/\; (1-\nu) \quad (12f)$$

$$D_{iT} = \int \zeta\, \alpha\, \tau\, E\, d\zeta \;/\; (1-\nu) \quad (12g)$$

In equations (12f) and (12g), τ is the local temperature change and α is the coefficient of thermal expansion.

The stiffness constants C_{ij}, K_{ij}, and D_{ij}, and the thermal forces and moments C_{iT} and D_{iT} are allowed to vary along the meridian. Equations (5) - (10) are 15 equations in terms of 15 unknowns N_s, N_θ, $N_{s\theta}$, M_s, M_θ, $M_{s\theta}$, e_s, e_θ, $e_{s\theta}$, k_s, k_θ, $k_{s\theta}$, u_s, u_θ, w. They may be combined in many ways to eliminate some of the intermediate variables. One such procedure is to reduce the system of equations to four simultaneous second-order differential equations (the three equilibrium equations and the fourth of equations (8-11)) following the concepts of reference (6). As indicated in reference (6) M_θ must be eliminated in such a way that k_s does not appear in order to prevent the appearance of derivitives of w higher than two. From the fourth and fifth of equations (11), the necessary relation can be obtained as

$$M_\theta = \frac{D_{12}}{D_{11}} M_s + \left[K_{12} - \frac{D_{12} K_{11}}{D_{11}}\right] e_s + \left[K_{22} - \frac{D_{12} K_{12}}{D_{11}}\right] e_\theta + \left[D_{22} - \frac{D_{12}^2}{D_{11}}\right] k_\theta + D_{2T} - \frac{D_{12}}{D_{11}} D_{1T} \tag{13}$$

and u_s, u_θ, w, and M_s are taken as the fundamental variables. The four simultaneous second-order differential equations can be written in matrix form as

$$Ez'' + Fz' + Gz + \bar{E}z'' + \bar{F}z' + \bar{G}z + E^*z'' + F^*z' + G^*z - \nu I\ddot{z} = e \tag{14}$$

where

$$z = \begin{Bmatrix} u_s \\ u_\theta \\ w \\ M_s \end{Bmatrix}, \quad \ddot{z} = \frac{\partial^2 z}{\partial t^2}, \quad I = \begin{bmatrix} 1 & 0 & 0 & 0 \\ 0 & 1 & 0 & 0 \\ 0 & 0 & 1 & 0 \\ 0 & 0 & 0 & 0 \end{bmatrix} \tag{15}$$

and E, F, G, $\bar{E}$, $\bar{F}$, $\bar{G}$, E^*, F^*, and G^* are 4 x 4 matrices. The barred and starred matrices contain the initial stress and deformation

CE-10

quantities and vanish if the initial state is a zero state. The starred quantities reflect the contribution of the square of the initial rotations on the behavior of the problem. Equation (14) may be applied to linear static stress analysis problems by setting the barred and starred quantities to zero and letting $\ddot{z} = 0$, applied to buckling problems by setting $\ddot{z} = e = 0$, and applied to prestressed vibration problems with $e = 0$, and assuming z harmonic in time.

E. Boundary Conditions

In Sanders' nonlinear theory, the conditions to prescribe on the edge of a shell of revolution are

$$\begin{array}{ll} N_s \text{ or } U & \hat{N}_{s\theta} \text{ or } V \\ \hat{Q}_s \text{ or } W & M_s \text{ or } \Phi_s \end{array} \tag{16}$$

where $\hat{N}_{s\theta}$ and $\hat{Q}_s$ are the effective shear and transverse forces per unit length defined by

$$\hat{N}_{s\theta} = N_{s\theta} + (3\, R_\theta^{-1} - R_s^{-1})M_{s\theta}/2 + \underline{(N_s + N_\theta)\, \Phi\, /2} \tag{17}$$

$$\hat{Q}_s = Q_s + M_{s\theta}^{\cdot}/r - \underline{\Phi_s\, N_s - \Phi_\theta N_{s\theta}} \tag{18}$$

Using the equilibrium equation (9) to eliminate Q_s from equation (18) leads to

$$\hat{Q}_s = [(rM_s)' + 2M_{s\theta}^{\cdot} - r'M_\theta]/r - \underline{\Phi_s N_s - \Phi_\theta N_{s\theta}} \tag{19}$$

Elastic restraints at the edge of a shell can be provided for by linearly relating the forces or moment to the appropriate displacements or rotation. Consequently, the boundary conditions may be given in the matrix form

$$\left[\bar{\Omega}\right]\begin{Bmatrix} N_s \\ \hat{N}_{s\theta} \\ \hat{Q}_s \\ \Phi_s \end{Bmatrix} + \left[\bar{\Lambda}\right]\begin{Bmatrix} U \\ V \\ W \\ M_s \end{Bmatrix} = \ell \tag{20}$$

where $\bar{\Omega}$ and $\bar{\Lambda}$ are 4x4 matrices and ℓ is a column matrix. The values of the elements of these matrices are determined by the conditions prescribed at the shell boundary. Procedures have been developed for independent boundary conditions of an uncoupled Fourier harmonic distribution. For the present case, however, simultaneous boundary conditions are imposed.

F. Ring Stiffeners

Circumferential ring stiffeners can be simulated at an arbitrary location along the shell. It is assumed that the ring has principal moments of inertia I_{rx} and I_{ry} about the centroidal axes which are perpendicular and parallel, respectively, to the axis of revolution. Further, the cross-sectional area, A, eccentricity, $\bar{e}$, and torsional constant, GJ, of the ring are specified. The basic problem is to determine the governing field equations of a ring that are compatible with Sander's shell equations.

Cohen[7] and Bushnell[8] have presented the generalized stiffness of rings. Weeks and Walz[9] illustrate a more thorough discussion when the centroid and shear center of the ring do not coincide. The above authors use the energy approach to derive the stiffness of the ring.

When the centroid and shear center are assumed to coincide and plane normal sections are assumed to remain plane and

normal during deformation, the ring strain energy is given by

$$\tilde{U}_r = \frac{r_c}{2} \int_0^{2\pi} \int^A \sigma_r \, (\bar{\varepsilon}_r - \alpha_T \, T) \, dA \, d\theta + \frac{1}{2} \frac{GJ}{r_c} \int_0^{2\pi} (\dot{\phi}_s + \frac{\dot{U}}{r_c})^2 \, d\theta \tag{21}$$

The hoop stress is defined to be

$$\sigma_r = E_r \, (\bar{\varepsilon}_r - \alpha_T \, T) \tag{22}$$

and the strain is defined by

$$\bar{\varepsilon}_r = \varepsilon_r - X \, k_x + Y \, k_y \tag{23}$$

The strain energy for the ring is therefore expressed:

$$\tilde{U}_r = \frac{r_c}{2} \int_0^{2\pi} \varepsilon_r^2 \, EA + k_x^2 \, EI_{ry} + k_y^2 \, EI_{rx} - 2 \, k_x \, k_y \, EI_{rxy} + \frac{GJ}{r_c^2} (\dot{\phi}_s + \dot{U}_r/r_c)^2 + 2 \, [\varepsilon_r \, N_r^T - k_x \, M_y^T + k_y \, M_x^T] \, d\theta \tag{24}$$

Where, the thermal loads are defined by

$$N_r^T = - \int^A E_r \, \alpha_r \, T \, dA \tag{25a}$$

$$M_y^T = - \int^A E_r \, \alpha_r \, X \, dA \tag{25b}$$

$$M_x^T = - \int^A E_r \, \alpha_r \, Y \, dA \tag{25c}$$

CE-13

Anamet Laboratories, Inc.

P.O. BOX 831, SAN CARLOS, CALIFORNIA 94070

and the strain displacement relations are

$$\left.\begin{aligned}
\varepsilon_r &= \dot{V}_r/r_c + W_c/r_c + \frac{1}{2}\,(\phi^2_{sr} + \phi^2_{\theta r}) \\
k_x &= \dot{\phi}_{\theta r}/r_c \qquad ; \qquad k_y = -\,\dot{\phi}_{\theta r}/r_c \;\ominus\; \phi_s/r_c \\
\phi_{sr} &= (\dot{W}_r - V_r)/r_c \\
\phi_{\theta r} &= \dot{U}_r/r_c
\end{aligned}\right\} \qquad (26)$$

The kinetic energy of a discrete ring is given by

$$T_r = \rho_r\left(\frac{r_c}{2}\right)\int_0^{2\pi} [A\,(U^2_{r,t} + V^2_{r,t} + W^2_{r,t}) + I_p\,\phi^2_{s,t} + I_y\,\phi^2_{sr,t} + I_x\,\phi^2_{\theta r,t} - 2\,I_{xy}\,\phi_{sr,t}\,\phi_{\theta r,t}]\,d\theta \qquad (27)$$

From the variational principle, the derivatives with respect to each of the fundamental variables will develop the stiffness and mass matrices.

The stiffness matrix is defined for a given Fourier harmonic, n, response by

$$G = \frac{E}{r_c^2}\begin{bmatrix}
\frac{n^2}{r_c^2}\left(n^2 I_x + \frac{GJ}{E}\right) & \frac{n^4}{r_c^2} I_{xy} & \frac{n^3}{r_c^2} I_{xy} & -\frac{n^2}{r_c}\left(I_x + \frac{GJ}{E}\right) \\
 & A + \frac{n^4 I_y}{r_c^2} & n\left(A + \frac{n^2}{r_c^2} I_y\right) & -\frac{n^2 I_{xy}}{r_c} \\
\text{Symmetric} & & n^2\left(A + \frac{I_y}{r_c^2}\right) & -\frac{n^2 I_{xy}}{r_c} \\
 & & & I_x + n^2\frac{GJ}{E}
\end{bmatrix} \qquad (28)$$

CF-14

Anamet Laboratories, Inc.

P.O. BOX 831, SAN CARLOS, CALIFORNIA 94070

not dimensionally correct

Mass matrix does not agree with stiffness matrix layout

and the mass matrix

$$\bar{\mu} = \frac{\rho}{r_c t} \begin{bmatrix} r_c^2 A + n^2 I_{\bar{y}} & n\, I_{xy} & n^2 I_{xy} & 0 \\ & r_c^2 A + I_x & n\, I_x & 0 \\ \text{Symmetric} & & r_c^2 A + n^2 I_x & 0 \\ & & & r_c^2 (I_x + I_y) \end{bmatrix} \begin{matrix} u \\ v \\ w \\ \phi_s \end{matrix} \tag{29}$$

The displacements and the rotation of the ring are related to a point on the shell's reference surface at the ring attachment by

$$\left.\begin{aligned} U_r &= U - e_1 \Phi_s \\ V_r &= -e_2/r_c\, \dot{U} + V\,(1 + e_1/r_c) - e_1/r_c\, \dot{W} \\ W_r &= W + e_2 \Phi_s \\ \Phi_r &= \Phi_s \end{aligned}\right\} \tag{30}$$

where the eccentricities of the ring to the shell are e_1 and e_2 in the X and Y direction, respectively.

For prismatic rings the force-displacement relations are noted to be

$$\left.\begin{aligned} N_{\theta_r} &= \frac{EA}{r_c}\,(\dot{V}_r + W_r) \\ M_{\theta_r} &= \frac{EI}{r_c^2}\,(-\ddot{W}_r + \dot{V}_r) \\ M_{t_r} &= \frac{GJ}{r_c}\,(-W_r'^{\cdot} - \dot{U}_r/r_c) \end{aligned}\right\} \tag{31}$$

With the definition of $\Phi_s = W_r'$, and by substituting equation (28) which represents the stiffness into equation (14), the ring can be easily introduced into the overall equilibrium of the shell.

Anamet Laboratories, Inc.

P.O. BOX 831, SAN CARLOS, CALIFORNIA 94070

III METHOD OF SOLUTION

A. Fourier Expansions

The crux of the method used here to solve the nonlinear field equations is the elimination of the independent variable θ by expanding all dependent variables into sine or cosine series in the circumferential direction. Only loading and initial conditions that are symmetric about a datum meridian plane will be considered. Thus, the variable Φ_s can be expressed in the form*

$$\Phi_s = \frac{\sigma_o}{E_o} \sum_{n=0}^{\infty} \phi_s^{(n)} \cos n\theta \tag{32}$$

where σ_o is a reference stress level, E_o is a reference elastic modulus, and the nondimensional series coefficient $\phi_s^{(n)}$ is a function of the independent variables s and T. Similar series expansions can be made for the remaining dependent variables.

B. Modal Uncoupling

In order to eliminate the independent variable θ from the problem, and convert the partial differential equations to sets of uncoupled partial differential equations, the nonlinear terms are treated as known quantities or pseudo loads. Since every nonlinear term is the product of two Fourier series, each product can be reduced to a single trigonometric series wherein the coefficient is itself a series. For example, using equation (32), ϕ_s^2 can be expressed as

$$\phi_s^2 = \left(\frac{\sigma_o}{E_o}\right)^2 \sum_{m=0}^{\infty} \sum_{n=0}^{\infty} \phi_s^{(m)} \phi_s^{(n)} \cos m\theta \cos n\theta \tag{33}$$

*Theoretically, the complete Fourier series including both the sine and cosine expansions should be used because of the possibility of "odd" displacements occurring under "even" loads, i.e., a bifurcation phenomenon. This aspect is not considered here for the nonlinear case.

See Appendix "F"

CE-16

Anamet Laboratories, Inc.

P.O. BOX 831, SAN CARLOS, CALIFORNIA 94070

Since

$$\cos m\theta \cos n\theta = \frac{1}{2}[\cos (m-n)\theta + \cos (m+n)\theta] \tag{34}$$

equation (18) can be given in the form

$$\phi_s^2 = \frac{\sigma_o}{E_o} \sum_{n=0}^{\infty} \beta_s^{(n)} \cos n\theta \tag{35a}$$

where

ABSOLUTE VALUE

$$\beta_s^{(n)} = \frac{\sigma_o}{2E_o} \sum_{i=0}^{\infty} \phi_s^{(i)} [\eta\, \phi_s^{(i+n)} + \mu\, \phi_s^{(|i-n|)}] \tag{35b}$$

with

$$\eta = \begin{cases} 0 \text{ for } n = 0 \\ 1 \text{ for } n > 0 \end{cases}, \quad \mu = \begin{cases} 1 \text{ for } i \neq n \\ 2 \text{ for } i = n \end{cases}$$

Similar series expressions can be derived for the other nonlinear terms in equations (5), (8), (17), and (18b). They are

$$\left.\begin{aligned}
\phi_\theta^2 &= \frac{\sigma_o}{E_o} \sum_{n=0}^{\infty} \beta_\theta \cos n\theta \\
\phi^2 &= \frac{\sigma_o}{E_o} \sum_{n=0}^{\infty} \beta \cos n\theta \\
\phi_s\phi_\theta &= \frac{\sigma_o}{E_o} \sum_{n=1}^{\infty} \beta_{s\theta} \sin n\theta \\
\phi_s N_s &= \sigma_o h_o \sum_{n=0}^{\infty} \eta_{ss} \cos n\theta \\
\phi_\theta N_{s\theta} &= \sigma_o h_o \sum_{n=0}^{\infty} \eta_{\theta s} \cos n\theta \\
\phi\, N_s &= \sigma_o h_o \sum_{n=1}^{\infty} \eta_s \sin n\theta
\end{aligned}\right\} \tag{35c}$$

CE-17

$$\left.\begin{aligned} \phi N_\theta &= \sigma_o h_o \sum_{n=1}^{\infty} \eta_\theta \sin n\theta \\ \phi_\theta N_0 &= \sigma_o h_o \sum_{n=1}^{\infty} \eta_{\theta\theta} \sin n\theta \\ \phi_s N_{s\theta} &= \sigma_o h_o \sum_{n=1}^{\infty} \eta_{s\theta} \sin n\theta \end{aligned}\right\} \qquad (35c)$$

where h_o is a reference thickness.

As a result of the trigonometric series expansions, there is one set of governing equations for each value of n considered; when only the linear terms are considered the sets are uncoupled. The presence of the nonlinear terms couples the sets through terms like $\beta_s^{(n)}$ as given by equation (35). However, by treating the nonlinear terms as known quantities and grouping them with the load terms, the sets of equations become uncoupled.

C. Spatial Finite Difference Formulation

Let the shell meridian be divided into K - 1 equal increments, and denote the end of each increment or station by the index i. Thus, i = 1 corresponds to the initial edge of the shell and i = K corresponds to the final edge. One fictitious station is introduced off each end of the shell at i = 0 and i = K + 1.

Let the first and second derivatives of z at station i be approximated by

$$z_i' = (z_{i+1} - z_{i-1})/2\Delta \qquad (36a)$$

$$z_i'' = (z_{i+1} - 2z_i + z_{i-1})/\Delta^2 \qquad (36b)$$

where Δ is the nondimensional distance between stations. Substituting equations (36a) and (36b) into equation 14 leads to

$$A_i\, z_{i+1} + B_i\, z_i + C_i\, z_{i-1} = g_i + 2\Delta\bar{\mu}_i\, (\partial^2 z/\partial t^2)_i \tag{37a}$$

where

$$\begin{aligned} A_i &= 2E_i/\Delta + F_i \\ B_i &= -\,4E_i/\Delta + 2\,\Delta\, G_i \\ C_i &= 2E_i/\Delta - F_i \\ g_i &= 2\,\Delta\, e_i \quad ; \quad \bar{\mu}_i = \nu\, I \end{aligned} \tag{37b}$$

and $i = 1, 2 \ldots K$ to insure equilibrium over the total length of the shell.

At the boundaries equation (20) must be satisfied. Thus, substituting equation (36a) into equation (14) leads to

$$\frac{1}{2\Delta}\,\Omega_1 H_1 z_2 + (\Omega_1 J_1 + \Lambda_1) z_1 - \frac{1}{2\Delta}\,\Omega_1 H_1 z_0 = \ell_1 - \Omega_1 f_1 \tag{38a}$$

at the initial edge, and

$$\frac{1}{2\Delta}\,\Omega_K H_K z_{K+1} + (\Omega_K J_K + \Lambda_K) z_K - \frac{1}{2\Delta}\,\Omega_K H_K z_{K-1} = \ell_K - \Omega_K f_K \tag{38b}$$

at the final edge.

For many cases, a shell structure comprised of composite elements develop discontinuity stresses near their juncture point. For example, a discontinuity in the membrane stress resultants will occur at the juncture of a cylindrical and spherical shell. In order to more accurately determine the stress distribution near these discontinuities, the mesh distribution must be finer than those areas away from the juncture.

A variable mesh spacing is represented at station i

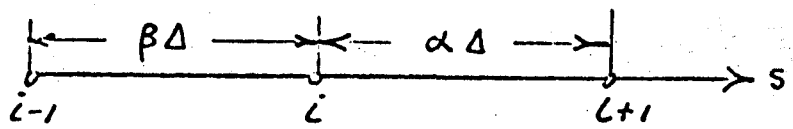

Let $\beta\Delta$ = Ratio $(i-1)\Delta_L$ and $\alpha\Delta$ = Ratio $(i)\Delta_L$, where Δ_L is the mesh spacing at the last station. From a Taylor's series expansion

$$Z_{i+1} = Z_i + \alpha\Delta\, Z_i' + \frac{(\alpha\Delta)^2}{2!} Z_i'' + \frac{(\alpha\Delta)^3}{3!} Z_i''' + \cdots \tag{39a}$$

$$Z_{i-1} = Z_i - \beta\Delta\, Z_i' + \frac{(\beta\Delta)^2}{2!} Z_i'' - \frac{(\beta\Delta)^3}{3!} Z_i''' + \cdots \tag{39b}$$

Multiplying the first by β^2 and the second by α^2 we obtain for the first derivative

$$Z_i' = \frac{1}{(\beta+\alpha)\alpha\beta\Delta}\left[\beta^2 Z_{i+1} + (\alpha^2 - \beta^2) Z_i - \alpha^2 Z_{i-1}\right] \underbrace{- \frac{\alpha\beta\Delta^2}{6} Z_i'''}_{O(\Delta^2)} \tag{40}$$

and for the second derivative

$$Z_i'' = \frac{2}{(\alpha+\beta)\alpha\beta\Delta^2}\left[\beta Z_{i+1} - (\beta+\alpha) Z_i + \alpha Z_{i-1}\right] \underbrace{- \frac{2(\alpha-\beta)\Delta}{3!} Z_i'''}_{O(\Delta)} \tag{41}$$

Since the error term in the second derivative is of order Δ, a variable mesh spacing through the discontinuity should not take place. Errors will occur at the juncture of the variable mesh. If the bending is low in these regions, no significant error in the solution should occur.

Lab. No. 173.01
January 4, 1973

A COMPUTER PROGRAM for the EVALUATION of SPECTRUM ACCELERATION USING FFT TECHNIQUES

By
Ray Bieber

Anamet Laboratories, Inc.
P. O. Box 831
San Carlos, California 94071

CE-21

I Introduction

In displaying the transient response of a structure to time-dependent loading, there are two primary choices available. One is to use the actual time history or "signature" of the measured or predicted quantity as the best index of the response characteristics. Secondly, some type of spectral representation which shows the predominate frequency content of the signal can be constructed. The use of the FFT for spectrum transient ground acceleration evaluation had been earlier proposed by Citerley[1]. In the present study the computation of an acceleration spectrum from transient data using the Fast Fourier Transform (FFT) algorithm is presented. The end result is a Fortran IV Digital Computer program for implementing the solution. The program was developed for use as a post-processor in analyzing the displacement output from a shell of revolution code; however it can also be used as a general purpose signal analysis routine.

Amanet Laboratories, Inc.

P.O. BOX 831, SAN CARLOS, CALIFORNIA 94070

II Analysis

A. Continuous Solution

The acceleration spectrum equations will be shown in "continuous" form and then restated for digital computation. For discussion purposes, the signal to be analyzed is a finite acceleration time history $\ddot{X}_o(t)$, continuous in the interval $0 \leq t \leq T$, and identically zero outside. The frequency content of $\ddot{X}_o(t)$ in a narrow range centered at frequency ω_n can be examined by considering the solution of,

$$\ddot{X}(t) + 2\,\xi\,\omega_n\,\dot{X}(t) + \omega_n^2\,X(t) = -\,\ddot{X}_o(t) \tag{1}$$

which is the response of a lightly damped ($\xi \ll 1.0$) single-degree-of-freedom spring-mass system to base acceleration, $\ddot{X}_o(t)$. The solution of (1) for the acceleration response, $\ddot{X}(t)$, can be expressed in integral form as,

$$\begin{aligned} \ddot{X}(t) &= \int_0^t h\,(t-\tau)\,\ddot{X}_o(\tau)\,d\tau \\ &= \omega_n \int_0^t e^{-\xi\omega_n(t-\tau)} \sin\,[\omega_n(t-\tau)]\,\ddot{X}_o(\tau)\,d\tau \end{aligned} \tag{2}$$

The above solution assumes zero initial conditions in X and $\dot{X}$.

The acceleration spectrum of $\ddot{X}_o$ will be defined as the maximum absolute value of $\ddot{X}$, i.e.

$$\begin{aligned} S_{\ddot{X}_o}(\omega_n;\xi) &= \mathrm{MAX}\ \{\,\mathrm{ABS}\,[\,\ddot{X}(t)\,]\} \\ &= \mathrm{MAX}\ \{\,\mathrm{ABS}\,[\,\omega_n \int_0^t e^{-\xi\omega_n(t-\tau)} \sin\,\omega_n(t-\tau)\,\ddot{X}_o(\tau)\,d\tau\,]\} \end{aligned} \tag{3}$$

Agbinet Laboratories, Inc.

P.O. BOX 831, SAN CARLOS, CALIFORNIA 94070

The argument $(\omega_n;\xi)$ denotes that $S_{\ddot{X}_o}$ is a function of ω_n and parameter, ξ. The selected values of ξ will usually be on the order of 0, .05, - - - .20.

Defining the Fourier transform of X(t) as,

$$X(i\omega) = \int_0^\infty X(t)\, e^{i\omega t}\, dt \tag{4}$$

then a transform solution for $\ddot{X}$ can be obtained. Taking the transform of both sides of (2) and applying the well-known convolution theorem, the following is obtained,

$$\ddot{X}(i\omega) = h(i\omega)\, \ddot{X}_o(i\omega)$$

$$\equiv \frac{\omega^2\, \ddot{X}_o(i\omega)}{\omega_n^2 - \omega^2 + 2\,\xi\,\omega_n\,\omega i} \tag{5}$$

Taking the Inverse Fourier Transform of both sides,

$$\ddot{X}(t) = \ddot{X}^{-1}(i\omega) = \left[\frac{\omega^2\, \ddot{X}_o(i\omega)}{\omega_n^2 - \omega^2 + 2\,\xi\,\omega_n\,\omega i} \right]^{-1} \tag{6}$$

where, the inverse transform is defined as

$$X(t) = X^{-1}(i\omega) = \frac{1}{\pi}\int_0^\infty X(i\omega)\, e^{-i\omega t}\, d\omega \tag{7}$$

Thus in terms of Fourier transforms the acceleration spectrum can be expressed,

$$S_{\ddot{X}_o}(\omega_n;\zeta) = \mathrm{MAX}\ \{\ \mathrm{ABS}\ [\ \ddot{X}(t)\ ]\ \} \tag{8}$$

$$= \mathrm{MAX}\ \{\ \mathrm{ABS}\ \left[\frac{1}{\pi}\int_0^\infty \frac{\omega^2\, \ddot{X}_o\,(i\omega)\, e^{-i\omega t}\, dt}{\omega_n^2 - \omega^2 + 2\,\zeta\,\omega_n\, i}\right]\}$$

B. Digital Solution

The most common method of solving for $\ddot{X}(t)$ is by numerical integration of equation (2), e.g. Simpson's rule. With the development of the Fast Fourier Transform (FFT) Algorithm, (see for example Ref. 2), it can be shown that it is numerically more efficient to use the transform form of the solution i.e. equation (6). Two digital solutions of the acceleration spectrum will be presented; one where the displacement signal $X_0(t)$ is given and the other where the acceleration $\ddot{X}_0(t)$ is given.

Using the notation and the definitions from Ref. 3, the FFT of the digital time series $X(t)$, $t=0, 1, - - - -, N-1$, is given by

$$X(\hat{t}) = \sum_{t=0}^{N-1} X(t) \; e^{\frac{2\pi i t \hat{t}}{N}} \tag{9}$$

Notice that the units of frequency are now Hz rather than Rad/sec as in the previous section i.e.

$$\omega = 2\pi f \tag{10a}$$

$$\omega_n = 2\pi f_n \tag{10b}$$

The time interval is $\Delta t = T/N$ and the frequency interval is $\Delta f = 1/T = 1/N\Delta t$. The highest frequency is $N\Delta f = 1/\Delta t$ which is the digital sampling rate. Thus there are an equal number, N, time ordinates and frequency ordinates. The inverse FFT of $X(\hat{t})$ is given by,

$$X(t) = \frac{1}{N} \sum_{\hat{t}=0}^{N-1} X(\hat{t}) \cdot e^{-\frac{2\pi i t \hat{t}}{N}} \tag{11}$$

Anamet Laboratories, Inc.

P.O. BOX 831, SAN CARLOS, CALIFORNIA 94070

One additional discrete transform theorem (Ref. 3) for finite difference derivatives is needed.

$$\sum_{t=0}^{N-1} \frac{\Delta X(t)}{\Delta t} e^{\frac{2\pi i t\hat{t}}{N}} = \frac{1}{\Delta t} \left(e^{\frac{-2\pi i \hat{t}}{N}} - 1\right) X(\hat{t}) \tag{12}$$

$$\text{where:} \quad \Delta X(t) = X(t+1) - X(t) \tag{12a}$$

Thus (12) gives the Fourier transform of the forward difference derivative of the function, $X(t)$.

The discrete transform solution of equation (6) can now be written,

$$\ddot{X}(t) = \frac{1}{N} \sum_{\hat{t}=0}^{N-1} \frac{f^2 \ddot{X}_o(\hat{t}) e^{\frac{-2\pi i t\hat{t}}{N}}}{f_n^2 - f^2 + 2\zeta f_n f i} \tag{13}$$

$$\text{where:} \quad f = \hat{t}\Delta f, \quad \hat{t} = 0, 1, - - - -, N-1 \tag{13a}$$

$$f_n = n\Delta f, \quad 0 \leq n \leq N-1$$

Substituting for f & f_n,

$$\ddot{X}(t) = \frac{1}{N} \sum_{\hat{t}=0}^{N-1} \left[\frac{\hat{t}^2}{n^2 - \hat{t}^2 + 2\zeta n\hat{t} i}\right] \ddot{X}_o(\hat{t}) e^{\frac{-2\pi i t\hat{t}}{N}} \tag{14}$$

The computational procedure for solving (14) is:

(1) Solve for $\ddot{X}_o(\hat{t})$ given the input signal, $\ddot{X}_o(t)$

(2) Multiply $\ddot{X}_o(\hat{t})$ by the complex filter function in the brackets

(3) Take the inverse transform of the complex product obtained in step (2).

For the case where the displacement of the signal is given rather than the acceleration, the derivative theorem of (12) is applied i.e.

$$\ddot{X}_o(\hat{t}) = \sum_{t=0}^{N-1} \frac{\Delta \dot{X}(t)}{\Delta t} e^{\frac{2\pi i t \hat{t}}{N}} \tag{15}$$

$$= \frac{1}{\Delta t^2} \left(e^{\frac{-2\pi i \hat{t}}{N}} - 1\right)^2 X(\hat{t})$$

Thus the computational procedure for solving (14), given the displacement, $X_o(t)$, is as follows:

(1) Solve for the transform, $X_o(\hat{t})$

(2) Compute $\ddot{X}_o(t)$ by (15)

(3) Multiply $\ddot{X}_o(t)$ by the complex filter function according to (14)

(4) Take the inverse transform of the complex product obtained in step (3).

The acceleration spectrum $S_{\ddot{X}_o}(\omega_n;\zeta)$ is easily solved from the definition, once the acceleration $\ddot{X}(t)$ is known.

Anamet Laboratories, Inc.

P.O. BOX 831, SAN CARLOS, CALIFORNIA 94070

III Computer Program

A computer program is described for evaluating the acceleration spectrum given either a displacement or acceleration signal. An arbitrary number of functions can be analyzed. The damping values and spectral frequencies are specified in the input data.

The FFT routine employed in computing the discrete transforms is that of Ref. 3*. The program will accomodate up to a 3-D complex function. Since the FFT technique relies on the length of the time series being of the form $N=2^n$, where n is an integer, the method of "filling out" with zeroes will be used. For example if a time series of length 1000 is given, then 24 zeros values will be added to form a new series of length $N = 2^{10} = 1024$.

The computer program is written in FORTRAN IV and is listed in Appendix A. A schematic of the solution for one input signal is shown in Fig. 1. The input time histories (displacement or acceleration) are analyzed sequentially. The input data format for each signal is given below.

Card 1 - Control Card

Format (3I5)

Col.		
1-5	IKIND	(1 for Displacement, 2 for Acceleration)
6-10	ND	(Unit Number of tape or drum for use in copying input or output data)
11-15	NL	(Length, number of data points in input signal)

---

*Other standard routines are available through SHARE.

Card 2 - Control Card

Format (6F10.0)

Col.

1-10	DELT	(Input record time interval, sec.)
11-20	ZETA	(Damping ratio, nondimensional)
21-30	FLO	(Acceleration spectrum lowest frequency required, Hz)
31-40	FHI	(Highest frequency required, Hz)
41-50	DF	(Frequency interval, Hz)
51-60	CONST	(Scale factor)

Card 3, - - -, N Data Cards

Format (8F10.0)

The card image form of the time series data can easily be changed to accommodate other formats. Also the time series data can be supplied on Unit ND via external control cards, so that handling of bulky cards is avoided.

END Card

Format (I5)

Col.

1-5 99999 (End of Data)

This card is supplied after all of the input signatures have been read and signals the end of the data deck.

In using the program and interpreting the spectral results, it must be remembered that the highest frequency component in the data to be analyzed must be less than 1/2 the highest FFT frequency, ($f_{max} = \frac{1}{\Delta t}$). If this is not the case, digital band-pass filtering of the raw data must be performed prior to spectral analysis. The latter can be easily accomplished using "autoregressive" or "moving average" techniques.

Anamet Laboratories, Inc.

P.O. BOX 331, SAN CARLOS, CALIFORNIA 94070

Figure 1 Flow Diagram for Calculation of Acceleration Spectrum for Displacement or Acceleration Input Record

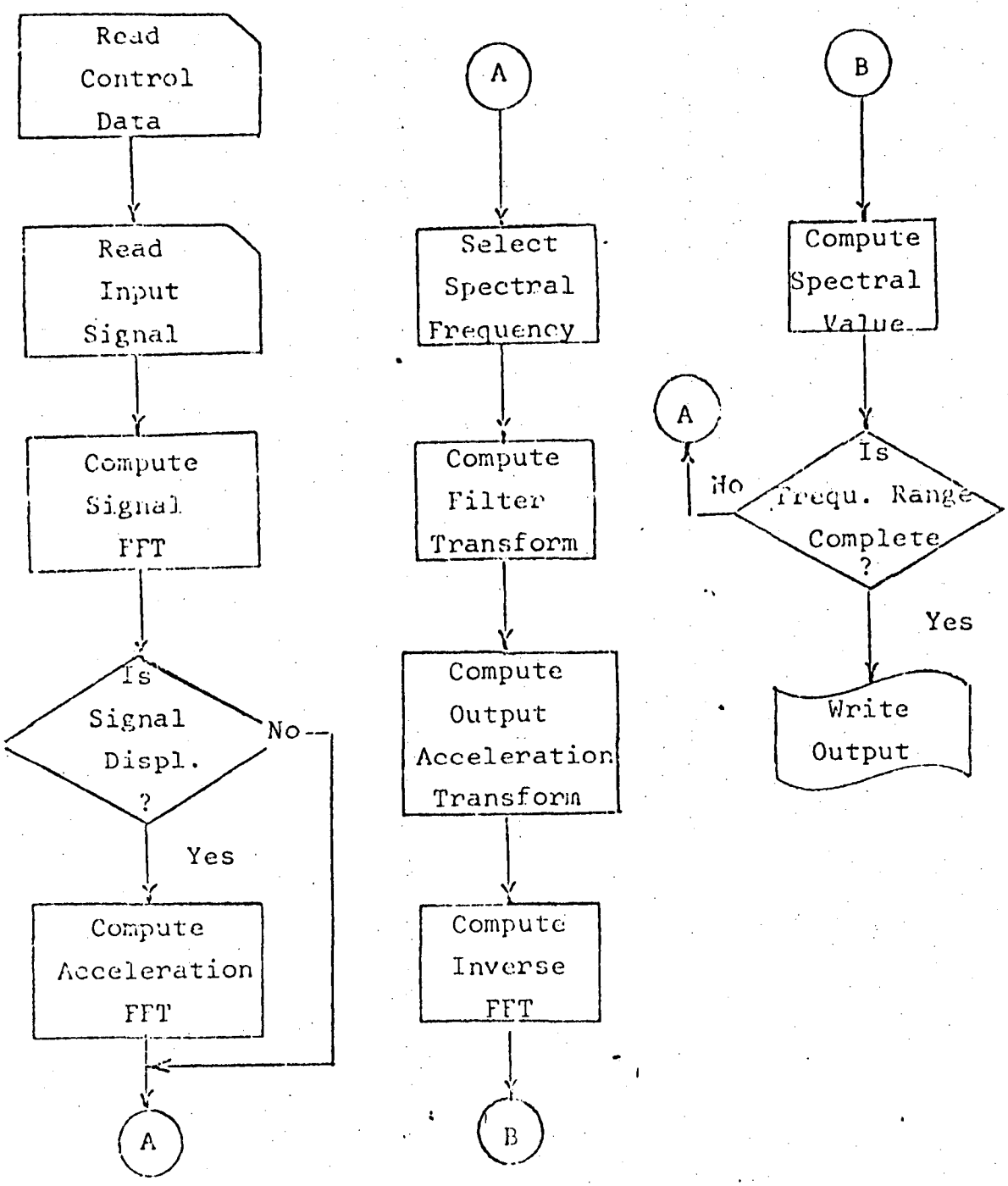

Anamet Laboratories, Inc.

P.O. BOX 931, SAN CARLOS, CALIFORNIA 94070

References

1. Citerley, R.L., Estimation of Ground Acceleration from Spectral Data, Anamet Report No. 470.259, April 1970.

2. Bergland, G.D., A Guided Tour of the Fast Fourier Transform, IEEE Transactions on Audio and Electroacoustics, June 1967.

3. Gentleman, W.M. and Sande, G., Fast Fourier Transforms - For Fun and Profit, Proceedings - Fall Joint Computer Conference, 1966.

CE-31

APPENDIX C

The Design of a Thin Shell Nuclear Containment Vessel for Seismic Loading

J. HAGSTROM
Assistant Manager,
Stress Analysis, Chicago
Bridge & Iron Co.,
Oak Brook, Ill. Mem. ASME

The Design of a Thin Shell Nuclear Containment Vessel for Seismic Loading

A procedure is presented for the design of a steel nuclear containment vessel subject to seismic loads. A design spectra representation of the loadings is used with a cantilever beam model of the vessel. The results for the beam model are compared with results from two independent shell analyses; a shell modal analysis and a nonlinear shell time history analysis. The beam results are shown to provide a good design correlation.

Introduction

The stringent safety requirements specified for the design of nuclear power facilities have, in recent years, led to increasingly comprehensive and sophisticated seismic design criteria. The following paper describes a design approach for a thin walled steel containment vessel using the modal analysis technique and a lumped mass cantilevered beam model of the vessel. The deflections and stress resultants calculated with this comparatively simple approach are compared with values determined with a modal analysis and a time history analysis using shell of revolution models of the containment structure. The beam results are found to provide good design correlation.

The techniques used for the shell of revolution models are described in a companion paper [1].[1] Only the results significant to a comparison for the various methods of analysis will be discussed in this paper.

The seismic response of containment structures has received considerable attention in the literature. Of particular interest are the experimental results reported in references [2] and [3]. In these experiments scale models of containment structures responded to simulated seismic loads in predominantly lobar modes with several waves around the circumference. This behavior is not in accordance with the assumptions inherent in using a beam model for the containment vessel, and the results gave incentive for a comparative nonlinear shell analysis.

Design Approach

The dimensions of the containment vessel under consideration are shown in Fig. 1. The vessel is considered to be free standing, supported only at the embedment point. The lumped mass idealization of the vessel is also shown in Fig. 1. The stiffness of the elastic elements joining the several masses are calculated in terms of the moment of inertia, area, and effective shear area of the vessel cross section. The calculation of the elements of the required stiffness matrix using a beam model with bending and shear flexibility is described by Pahl in [4]. Pahl shows that the stiffness terms calculated with beam theory and with membrane shell theory are identical for cylindrical shells if the beam moments of inertia are divided by $(1 - \nu^2)$ to account for the Poisson effect in the shell. It is because of this similarity with membrane shell theory that the beam model is applicable to relatively short cantilever structures such as the containment vessel in Fig. 1. The inclusion of the shear flexibility, not commonly considered for the vibration of longer beams, is a necessity in using the beam analogy for this vessel.

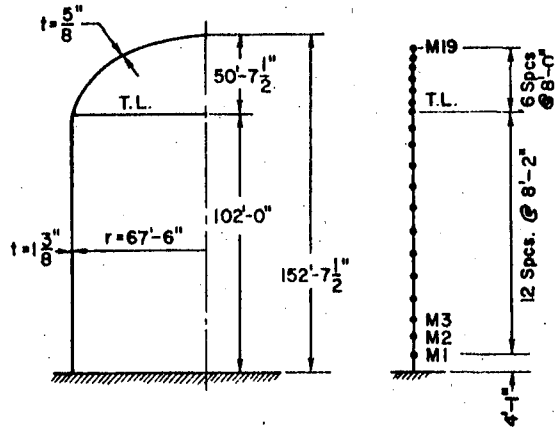

Fig. 1

[1] Numbers in brackets designate References at end of paper.

Contributed by the Pressure Vessel and Piping Division and presented at the Winter Annual Meeting, Washington, D. C., November 28–December 2, 1971, of The American Society of Mechanical Engineers. Manuscript received at ASME Headquarters, July 28, 1971. Paper No. 71-WA/PVP-10.

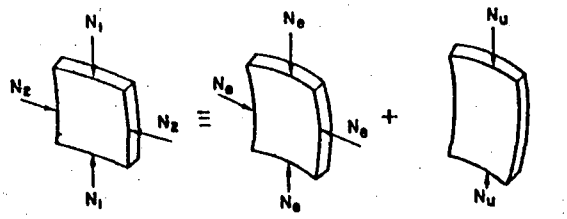

$$\frac{N_e}{N_{sphere}} + \frac{N_u}{N_{cylinder}} \leq 1$$

WHERE,

N_e IS THE SMALLER OF N_1 OR N_2.

N_u IS EQUAL TO THE DIFFERENCE $N_1 - N_2$.

N_{sphere}, $N_{cylinder}$ ARE ALLOWABLE COMPRESSIVE STRESS RESULTANTS IN SPHERE, CYLINDER.

Fig. 2 Unequal biaxial compression

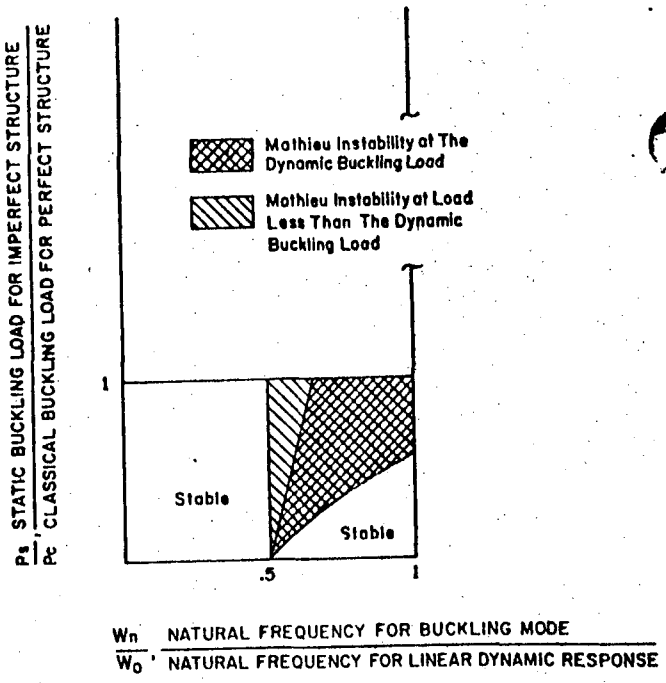

Fig. 3 Mathieu stability diagram for step loading taken from [5]

The stiffness properties for vertical displacements in the top head require special consideration. A static shell of revolution computer code is used here to develop the equivalent beam properties.

The seismic loadings for the operating basis earthquake (OBE) and design basis earthquake (DBE) are specified in terms of design spectra for the required range of structural frequencies. The horizontal ground motion represented by the design spectra produces rigid body translation of the shell embedment cross section. The radial and circumferential shell displacements can be expressed in terms of cosine and sine functions of the circumferential angle. The vertical ground motion can be described as axisymmetric movement of the embedment cross section. The inertial forces produced by the ground motion and the resulting vessel displacements and stresses can be described in terms of sine, cosine, and axisymmetric components unless significant nonlinear effects are present. In using membrane shell, or beam, theory the assumption is made that the vessel cross section is not significantly distorted by the applied loads, i.e., the type of behavior described in [2] and [3] does not occur or has no appreciable effect.

The structural frequencies, mode shapes, and modal response in terms of deflections, accelerations, shears, axial forces, and moments are determined in the usual manner. Longitudinal and shear stress resultants for the shell can be determined from the beam forces by statics, and the modal accelerations can be used to calculate the circumferential stress resultant and distortion of the vessel cross section as described later.

Design Criteria

The specified loading combinations for the containment vessel include seismic loading combined with dead load and external pressure. The thin shell geometry of the vessel dictates that stability considerations will govern the required shell thicknesses. The envelope of results calculated for the above combination of loads includes axisymmetric, sine and cosine components. In selecting a shell thickness, the maximum compressive meridional stress resultant in the cylindrical shell is limited to the allowable value given by the rules of Section III of the ASME Boiler and Pressure Vessel Code for uniform axial compression. The maximum compressive circumferential stress resultant is similarly limited to the value calculated from the allowable external pressure as given by the rules of Section III.

In the doubly curved vessel head the maximum circumferential and meridional stress resultants are separated into an equiaxial component equal to the smaller compressive value and an uniaxial component equal to the difference between the maximum and minimum compressive values, see Fig. 2. The sum of the ratios of the equiaxial component to the spherical compressive allowable and the uniaxial component to the cylindrical compressive allowable is limited to unity as indicated in Fig. 2. The spherical and cylindrical allowables are again determined from the rules of Section III using appropriate shell curvatures.

In using this buckling criteria, it is assumed that the compressive stress allowables for static axisymmetric loads give a conservative measure for the permissible maximum dynamic stresses for time varying nonaxisymmetric loads.

The stability of thin walled cylinders is sensitive to imperfections in geometry. The allowable static compressive stresses given by the rules of Section III reflect the decrease in the buckling load due to imperfections which are within Code fabrication tolerances. Budiansky [5] has shown that the essential imperfection characteristics of shell structures are revealed in the decrease in the static buckling load and separate consideration of the many possible imperfection combinations is not necessary for a large class of dynamic problems.

Using a nonlinear coupling of the modes to provide the mechanism, Budiansky also considers the transfer of total energy of a structure from a linear response mode to a buckling mode for dynamic loading. Such a mechanism could produce a lobar response of containment models even in the small deflection range. The investigation of this type of nonlinear energy transfer for small deflections (order of the shell thickness) leads to Mathieu type stability diagrams[2] as shown in Fig. 3. This plot is for a suddenly applied constant load and is taken from reference [5]. The diagram indicates that the pertinent stability parameters are the ratio of the static buckling load to the classical buckling load and the ratio of the natural frequency of the shell in the assumed buckling mode to the frequency in the linear response mode.

Because the Section III design rules give a static buckling load that is a small fraction, less than 1/3, of the classical buckling

[2] For example see [6].

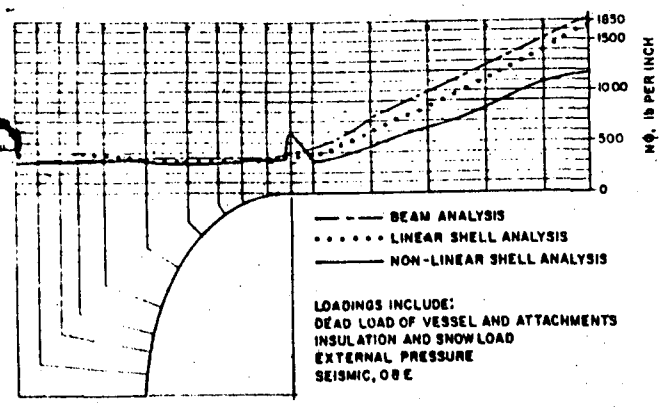

Fig. 4 Linear spectral stress resultants and maximum absolute values for nonlinear stress resultants, meridional direction

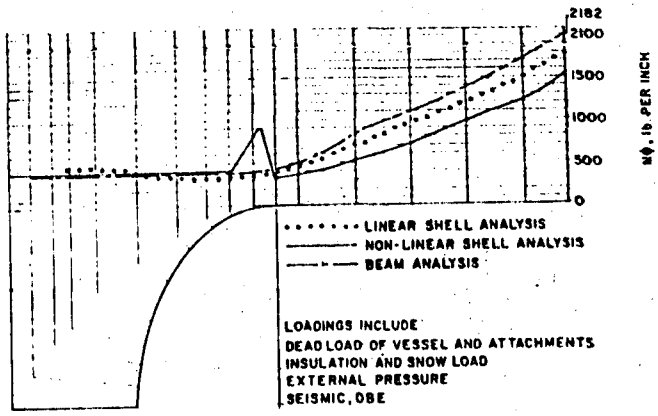

Fig. 6 Linear spectral stress resultants and maximum absolute values for nonlinear stress resultants, meridional direction

load, the region of instability of concern is for frequency ratios close to $^1/_2$. The low energy deformation modes for the vessel configuration under consideration involve ten to twelve circumferential waves. The ratio of the natural frequencies for these modes to the axisymmetric and sine and cosine linear response frequencies is less than $^1/_4$. Budiansky's approach indicates that nonlinear energy transfer from the linear response modes to the lowest energy buckling modes will not grow in an unbounded manner and lead to instability, at least not for a suddenly applied constant load. The results of the nonlinear time history analysis provide a more precise measure of this phenomenon for the specified seismic loadings and will be discussed later.

Results

The response of the model described above for the specified design spectra is predominantly in the first beam mode. For engineering purposes, the first three beam modes comprise the entire response. The vertical displacements and forces, the horizontal displacements and shears, and the moments acting on the beam model are determined from the design spectra for each mode considered using the appropriate participation factor. The total response is determined using a root mean square combination of the modes.

The circumferential stresses cannot be directly determined from the design spectra because of the simplifying assumptions made in developing the beam model. A conservative value for these stresses can be obtained using a static shell of revolution analysis with radial and circumferential loads equal to the unit area mass of the shell times the root mean square sum of the spectral accelerations. At points removed from shell discontinuities the circumferential stress resultant can be calculated directly with the membrane equations for cylindrical shells.

Comparison of Beam Results With Shell Solution

The beam approach involves a number of simplifying assumptions; and as previously mentioned, experimental investigations have exhibited responses substantially different from that predicted by the beam model. Therefore, an independent analysis of the seismic response of the containment vessel was made using an identical geometry and design spectra. In order to investigate the possibility of a lobar type response, a second shell of revolution analysis was made using nonlinear theory, a model of the vessel with initial imperfections, and an acceleration time history compatible with the design spectra.

The stress resultants calculated with the three methods, beam modal analysis, shell modal analysis, and shell nonlinear time history analysis, are shown in Figs. 4 through 7.[3] In plotting the results for the nonlinear time history analysis, the maximum values for the various parameters for the duration of the time history loading have been shown. These maxima do occur at different instances in time for the various parameters and cross sections of the vessel.

The plots of the stress resultants reveal that the beam model gives adequate and reliable results for the vessel configuration being considered. The beam results are consistently greater than the nonlinear shell time history results. This is in part due to the conservative approach used with the beam model and in part due to the fact that the specified design spectra curves lie above the envelope of maximum response calculated from the specified time history; the design spectra were drawn in a conservative manner.

The results of the nonlinear time history also indicate that the vessel is structurally stable when subjected to the specified load combination. Any instability or approach to an unstable con-

[3] Shell modal results and nonlinear time history results are taken from [7].

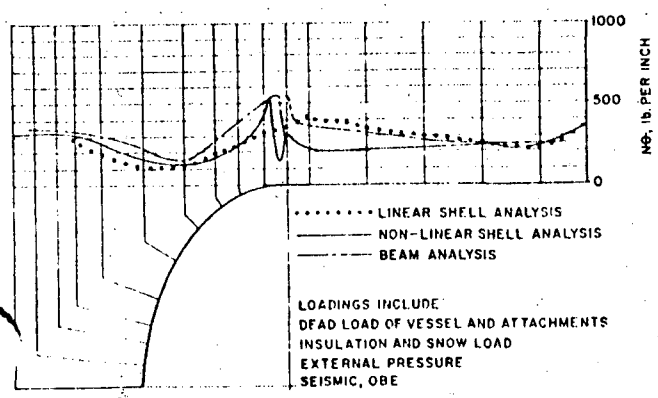

Fig. 5 Linear spectral stress resultants and maximum absolute values for nonlinear stress resultants, circumferential direction

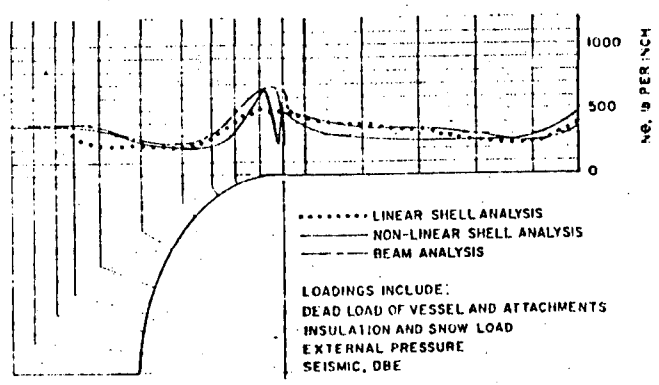

Fig. 7 Linear spectral stress resultants and maximum absolute values for nonlinear stress resultants, circumferential direction

figuration will show up as an increase in the number of iterations required for the solution of the nonlinear equations at a particular step in the time history.[4] While nonlinear effects are present for the specified loadings, no instability problems are encountered. This result demonstrates the adequacy of the design criteria for the geometry and loadings being considered.

Conclusions

The design of a steel containment vessel, $r/t \simeq 600$, $L/D \simeq 1$, for seismic loads using a beam model of the vessel with specified design spectra for OBE and DBE loads has been checked with independent shell spectral results and a nonlinear time history analysis. The beam approach gives stress resultants which are in agreement with the values calculated by the two independent methods. The dynamic design criteria developed from the static buckling criteria of Section III of the ASME Code produce a vessel configuration which remains stable during the nonlinear time history analysis. The criteria suggested by Budiansky [5] for evaluating the possible nonlinear coupling between linear dynamic response modes and low energy buckling modes is in agreement with the results of the nonlinear time history for the particualr geometry and loadings being considered.

The beam analogy, with shear flexibility, can provide a useful and adequate model for the linear seismic analysis of thin shell steel containment vessels.

[4] Reference [1] describes the nonlinear analysis in detail.

Acknowledgments

The foregoing work was done under contract to Bechtel Corporation, WADCO and the Atomic Energy Commission. Their permission to publish these results is appreciated. The shell modal and nonlinear time history results were provided by Anamet Laboratory. Anamet's contribution is gratefully acknowledged.

References

1 Citerley, R. L., and Ball, R. E., "Nonlinear Seismic Analysis of Thin Reactor Containment Vessels," companion paper published concurrently in this volume.

2 Arita, Y., Nakao, Y., Kimoto, K., Satake, M., and Katayama, M., "Study on Earthquake Resisting Strength of Nuclear Reactor Containment Vessels," Mitsubishi Heavy Industry Ltd., *Technical Review*, May 1968.

3 Toriumi, I., "Model Analysis of a Seismic Design of a Nuclear Reactor Building," *Nuclear Structural Engineering*, Vol. 2, No. 3, Sept. 1965, pp. 301–305.

4 Pahl, J. P., "Modal Response of Containment Structures," *Seismic Design for Nuclear Power Plants*, Hansen, R. J., ed., The M. I. T. Press, Cambridge, Mass., 1970, pp. 344–400.

5 Budiansky, B., and Hutchinson, J. W., "Dynamic Buckling of Elastic Structures: Criteria and Estimates," *Dynamic Stability of Structures*, Hermann, G., ed., Pergamon Press, 1967, pp. 83–106.

6 Goodier, J. N., and McIvor, I. K., "The Elastic Cylindrical Shell Under Nearly Uniform Radial Impulse," *Journal of Applied Mechanics*, Vol. 31, TRANS. ASME, Vol. 86, Series E, No. 2, June 1964, pp. 259–266.

7 "Nonlinear Seismic Analysis of the FFTF Containment Vessel," Anamet Laboratory Report #171.260, San Carlos, Cal., Jan. 1971, unpublished.

8 Biggs, J. M., *Introduction to Structural Dynamics*, McGraw-Hill, New York, 1964.

Reprinted from the August 1972
Journal of Engineering for Industry

APPENDIX D

Mass Loading Effects on Vibration of Ring and Shell Structure

SD 68-29

MASS-LOADING EFFECTS ON VIBRATION OF RING AND SHELL STRUCTURES

(CONTRACT NAS8-20019, PHASE III)

February 1968

Prepared by

S. Y. Lee
S. S. Tang
J. G. Liyeos

Approved by

S. Y. Lee, Project Engineer

F. C. Hung, Program Manager

Structures & Design Dept., Research, Engineering & Test

SPACE DIVISION
NORTH AMERICAN ROCKWELL CORPORATION

ABSTRACT

Efficient methods for predicting the effects of attached masses on the vibration characteristics of ring and shell structures were developed and substantiated with experimental data. Analytically, the series expansion technique was used in solving the mass-loaded shell problem, while both the finite-element and transfer-matrix methods were employed in the analysis of mass-loaded ring structures. Experimentally, aluminum ring and shell structures loaded with discrete masses were excited by a electrical induction force, and the vibratory motion was measured by an automatically revolving proximity gage. The influences of the masses of the exciter and of the instrumentation, thus, were eliminated. Response data were obtained with miniature accelerometers and with a proximity gage for comparison purposes. The studies show, in addition to the amplitude changes of the local vibration response caused by the addition of the discrete masses, the frequency shifts, the change of modal behavior, and the transmissibility characteristics resulting from the increased discrete mass on the structure. The results show (1) that the response attenuation for the first mode was somewhat similar to the procedure currently recommended by NASA/MSFC for predicting the amplitude reduction of the local vibration response of unloaded structure to account for the influence of the addition of the mass; (2) that for higher modes, much more amplitude reductions were found, and the rate of amplitude reduction progressed very rapidly; and (3) that the transmissibility characteristics in a function of normal modes, indicated some differences for beams, plates, honeycomb plates, rings, and shells.

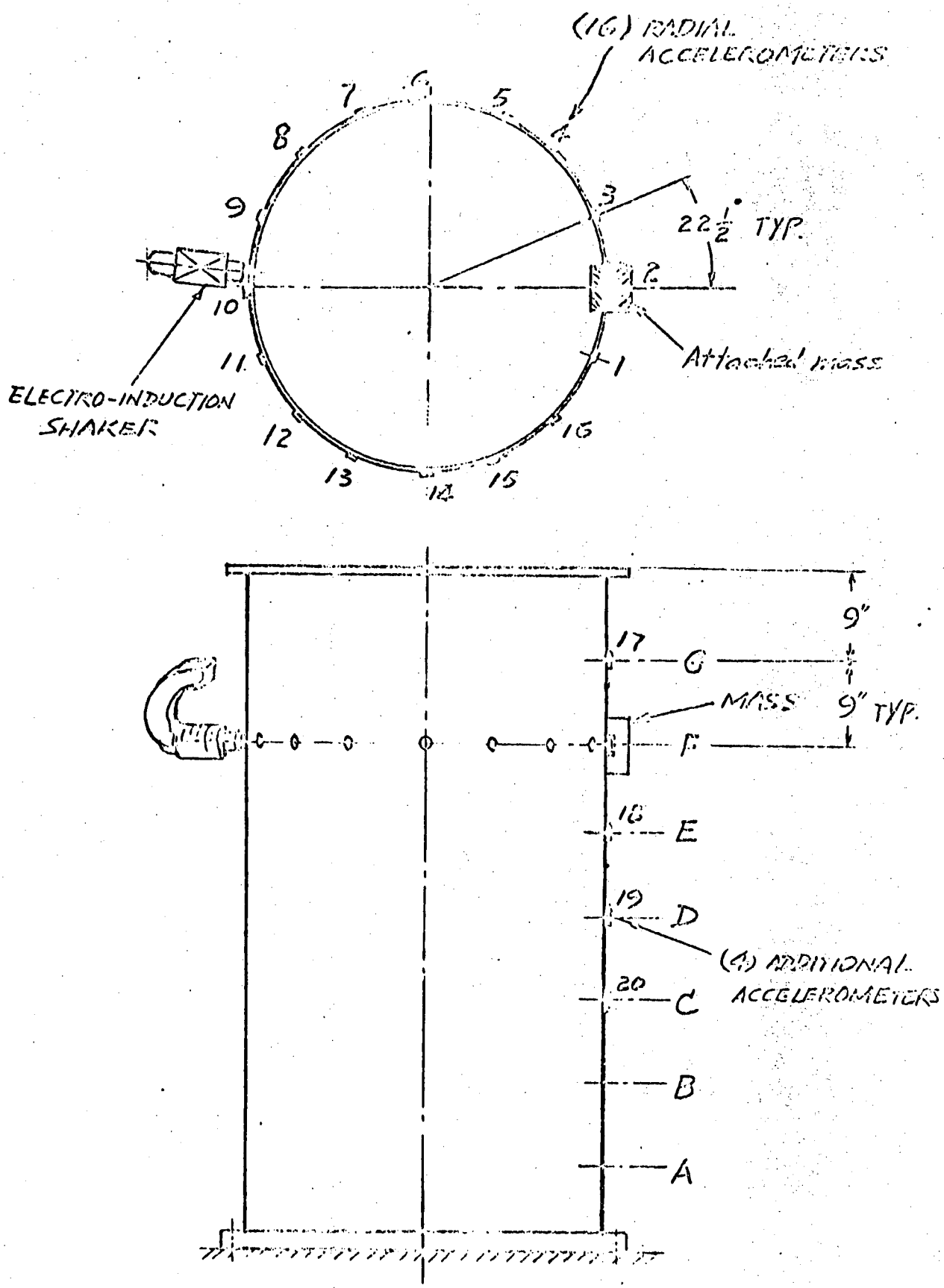

Figure 13. Accelerometers Set-up for Vibration Test of Mass-Loaded Shell

7.0 CONCLUSIONS

The analytical and experimental studies of the mass-loading effects on vibration of rings and shells can be summarized as follows:

1. Efficient methods have been developed for analyzing vibration of mass-loaded ring and shell structures.

2. Analytical results closely agreed with test data.

3. Frequency-shifts for mass-loaded rings and shells differed somewhat from those previously obtained in the Phases I and II of this program for the cases of beams and plates. Because of the motion of the mass interacted with the two- or three-dimensional motions of the support structures, the effect of mass loading on rings and shells caused a decrease in natural frequencies; however, for the higher modes, the frequency shifts became less significant as the attached mass increases. This information was presented in this report in the form of equations, tables, plots, and nondimensional graphs for various applications.

4. Transmissibilities and attenuations followed a trend similar to that of beams and plates, but possessed special characteristics. The results followed the equation $y = A + \frac{B}{X^n}$ which was previously established in Phases I and II of this program. The coefficients A, B, and n can be determined from the transmissibility plots in conjunction with firing test data and some consideration for design safety.

5. Mass loading also caused changes in mode shapes and disappearance of some modes at the mass mounting location; however, these phenomena of rings and shells deviated from that of beams and plates and were demonstrated by test data and computer solutions in this report.

6. The free vibration characteristics of mass-loaded shells can be solved analytically by the Fourier series-expansion technique,

which gives closed-form and nearly exact solution. This method required the use of four summations of the m n i j terms instead of only two summations of m n terms to describe the interacted motion.

7. Transfer matrix methods were efficient in calculating the lower frequencies of ring structures, while the finite-element method was good for both lower and higher frequencies. The transfer matrix method, however, offered a simple direct solution which provided a step-by-step insight into the solution and was helpful in the study of response characteristics.

8. The developed experimental and instrumentation techniques permitted continuous plotting of mode shapes and produced meaningful data for immediate evaluation during the test.

9. Sufficient data had been obtained for smaller mass ratios to better define the mass-loading phenomena.

As a general conclusion to the study, the trend of mass-loading effects on vibration of ring and shell structures has been established and the prediction methods have been developed; however, some refined studies and investigations for applications are needed and recommended as follows:

1. Refine the closed-form exact-solution technique for shell vibration analysis.

2. Further define the analysis of mass-loading effects on modal characteristics of shell structures.

3. Investigate the finite-element technique for obtaining an approximate solution for shell vibration.

4. Apply results to solve bracketry problems, definition of support structures, design of local structures, and test and evaluation of components.

5. Further refine the experimental technique.

6. Simplify the analytical solution, and reduce the mathematical complexity for further development in the definition of the basic mass-loading mechanism.

7. Extend the developed method to solve vibration problems of complicated shell structures loaded with bulkheads, propellants, ring frames, longerons, and a variety of discrete masses.

APPENDIX E

Effect of Nonsymmetric Thermal Loading on Shell

INTRODUCTION

This analysis has been performed to determine the stresses in the vessel due to the nonsymmetric thermal loading as prescribed in the TVA Specification for the Watts Bar Containment Vessel.

The shell temperature transients have been specified in Appendix C of the specification and represent average shell temperatures adjacent to the three compartments as a function of time after the design basis accident occurs.

The thermal stress analysis of the containment vessel is made using CBI computer program 781 which performs a linear analysis for any axisymmetric thin shell structure subjected to an arbitrary nonsymmetric loading.

The program considers that the distribution of the ambient temperature through the thickness of the shell is a linear variation. In this analysis it is assumed that no thermal gradient exists through the shell thickness.

In our analysis it is assumed that the ambient temperature at which the vessel was fabricated represents the initial condition. This reference temperature is taken as $T_1 = 70^oF$.

At time t = 1000 secs. after the design basis accident, the change in the ambient temperature from T_1 (70^oF) to T_2 (the average shell temperature for different compartments) is completed and it is assumed that this temperature remains constant. There is, however, a temperature distribution which exists both axially along the shell meridian at the elevation of the compartment "dividers" and circumferentially at boundaries between the compartments.

The program calculates stresses and deflections in the vessel due to the nonsymmetric temperature variation around the shell.

DESCRIPTION OF COMPUTER MODEL

The vessel has been idealized as an axisymmetric thin shell. The basic structural components are the vertical cylinder, hemispherical dome and circumferential stiffeners (Figure 1). The circumferential ring stiffener is considered as a cylinder of length "t_1" and thickness "b_1", (Figure 2). The stiffness of the ring out of its plane is assumed to be negligible.

The vertical stringers are accounted for in the analysis by use of an equivalent orthotropic layer described by an equivalent stiffness in the merdional direction and zero circumferential stiffness. The bending stiffness of the model is made equal to that of the actual structure by equating the stiffnesses EI

$$\bar{E}_\alpha \left\{ \frac{ad^3}{12} + ad\left(\frac{d}{2}\right)^2 \right\} = E_\alpha \left\{ \frac{bd^3}{12} + bd\left(\frac{d}{2}\right)^2 \right\}$$

where,

$\bar{E}_\alpha$ = modulus of elasticity of orthotropic layer

E_α = modulus of elasticity of actual structure at pertinent ambient temperature

a = average spacing of gussets

b = thickness of the vertical stringers

d = depth of vertical stringers

The above equation can be simplified to the form

$$E \quad \bar{E}_\alpha = E_\alpha \times \left(\frac{b}{a}\right)$$

The model consists of a total of 32 parts including 12 circumferential stiffeners and 20 shell panels.

Influence coefficients for the top crown region of the hemispherical head (as illustrated in Figure 3) which is not considered in the model are defined in the form of spring matrices at the end of the model. The stiffness matrices for the various harmonics are shown on page 15.

For the purpose of this analysis, the vessel is divided into three regions. The "Lower Compartment Region" extends from the embedment (elev. 702' - 9 3/8") to elev. 744' 6" which corresponds approximately to the elevation of the top surface of the vapor barrier between the ice condenser compartment and lower compartment (refer Figure 4).

The "Ice Condenser Region" is the region along shell meridian from elev. 744' 6" to elev. 805' 0" which is about 2' above the top of the ice bed (Figure 4).

The "Upper Compartment Region" comprises the cylindrical shell above elev. 805' 0" and spherical segment of the top head up to an angle equal to 40° from the spring line of the top head.

NONAXISYMMETRIC THERMAL LOAD REPRESENTATION

The temperature of the shell adjacent to the Ice Condenser is 53°F at time t = 1000 secs. The temperature of the shell adjacent to the Upper and Lower compartment are 140°F and 220°F respectively at t = 1000 sec. (Refer to Figure C-2 Appendix C of TVA Specification).

TEMPERATURE DISTRIBUTION IN LOWER COMPARTMENT REGION

Now since the lower compartment region is continuous around the complete periphery of the vessel from embedment to elev. 708' 0", the circumferential temperature distribution is taken as uniform in this region. The axial distribution of temperature in this region is determined from Figure C-1 of the TVA Specification. The shell temperature is taken as 80°F at embedment, increasing to 94°F over a height of 3' 9" (Elev. 706' 6"). Then a steep

rise in temperature from 94°F to 220°F occurs over the next 18" (Elev. 708' 0").

From elevation 708' to elevation 744' 6" the upper compartment extends over an arc region of 60° whilst the lower compartment extends over the remaining shell region (Azimuth 30° to 330°).

Hence in this region the distribution of temperature in the circumferential direction is nonsymmetric, 140°F from Azimuth 330° to 30° and 220°F from Az. 30° to 330°. This nonsymmetric temperature distribution is represented in the form of a Fourier cosine series using 9 terms as shown in figure 5 on page 13. Fourier coefficients for the 9 harmonics used to depict this temperature variation are shown on page 15.

The temperature distribution along the shell meridian in this region changes at two locations; one, in the vicinity of elevation 708' and the other is at the elevation where the ice condenser compartment barrier is situated (elev. 744'6"). The temperature change in the meridional direction at elev. 708' from 220°F to 140°F is assumed to occur over a distance of 6'. The temperature change in the axial direction at the elevation of the ice condenser barrier is assumed to take place over a distance of 18" (from elev. 743' to 744'6"), from 220°F in the lower compartment region to 53°F in the ice condenser region.

TEMPERATURE DISTRIBUTION IN ICE CONDENSER REGION

The temperature distribution for the shell in the ice condenser region is also nonsymmetric, 140°F from Azimuth 330° to 30° and 53°F from Azimuth 30° to 330°. This nonsymmetric temperature distribution is also represented in the form of Fourier cosine series as shown in Figure 6 and the Fourier coefficients

are as shown on page 15. This nonsymmetric temperature distribution extends into the Upper Compartment region for a distance of 6' up to elev. 811' which is about 8' above the top of ice bed. The shell above elevation 811' is assumed to be at a uniform temperature of 140°F around the complete circumference.

RESULTS

The numerical results of the analysis are presented in the form of plots. The plots are for the stresses and deformations along the shell meridian and also around the circumference (Azimuth 0° - 180°) at several pertinent locations.

The plots along the shell meridian are for the "Lower Compartment" region (origin at embedment) up to elevation 744'-6" plotted to a vertical height of 9" and also for the "Ice Condenser Region" (origin at elev. 744'-6") and extending to elevation 811'-0" plotted also to a vertical dimension of 9". Stresses are shown along the shell meridian at Azimuths 0°, 30°, 45°, 60° and 90°.

Stresses are also shown around the circumference of the shell (0° - 180° plotted to a dimension of 9") at several pertinent locations. The locations considered are the embedment elevation (702' - 9-3/8"), Elev. 708', elev. 719'-3-5/8" (centerline of lower personnel lock), elev. 743', elev. 744.5' (elevation at which ice condenser region starts), elev. of centerline of upper personnel lock (760' - 3-5/8"), elevation of centerline of equipment door (764' - 7-1/2") and elevation 805' (2' above top of ice bed).

Radial (normal to shell) displacement and longitudinal rotation as well as in-plane displacements (meridional and circumferential) are plotted for the two regions along the shell meridian for azimuths 0 and 30 degrees only. These deformations are also

plotted around the shell circumference at embedment level, centerline of locks and equipment door and at the end of the ice condenser region (elev. 805'-0").

At the bottom of each page, the maximum value of each variable which is plotted on that page is printed. The plots on any page are plotted ~~to~~ a scale based on making the max. value of the first variable printed at the bottom of the page equal to a dimension of 4" from the base line. If for any other plot on that page, this scale results in the maximum ordinate to exceed 4" then the scale for that plot is adjusted so that the max. ordinate is 4". Positive (tensile) values of the vectors (stresses and deformations) are plotted to the left of the base line while negative (compressive) values are to the right.

The stresses are plotted at the midsurface of the vessel wall (identifying symbol 0 on curve) and the inside (Δ) and outside surface ( ) of the shell. For the stress curves, the first, second and third values at the bottom of the page represent the maximum values for the inside surface, membrane and outside surface stress respectively.

The maximum longitudinal stress occurs in the region where the ice condenser compartment "barrier" is situated just below Elev. 744'6". The maximum values are 23175 psi (tension) on inside face and 22000 psi (comp.) on the outside face. The maximum longitudinal stresses at the embedment level are 17800 psi (tension) on outer surface and 16350 on inside surface.

The maximum circumferential stress also occurs in the ice condenser compartment "barrier" region just above Elev. 743'0". The maximum values are 15612 psi on inside and 14700 psi on outside, both compression. The maximum tensile circumferential stress occurs at about 2' above embedment. Its value is about 15400 psi on inside and outside face.

CBI

In the ice condenser region the stresses (both meridional and circumferential) are rather nominal. The maximum meridional stress is of the order of 15000 psi (tension) on the outside face. The maximum circumferential stress is of the order of 9200 psi (tension) on the inside face and 5300 psi (compression) on the outside face. These stresses occur at Elevation 744'6" which corresponds to the elevation where the ice condenser region starts.

Since the stresses due to temperature are less than 1½ Sm then the stresses due to the combined loads will be less than the allowable 3 Sm.